Ca' Foscari University of Venice

Master's Degree programme

in Environmental Sciences
Second Cycle (D.M. 270/2004)

Final Thesis

Cross scale evaluation of cooling effect ecosystem service by vegetation: understanding relationship with landscape and patch attributes for Green Infrastructure strategic planning

Supervisor
Ch. Prof. Gabriella BUFFA

Assistant supervisor
Dr Andrea DELLA BELLA

Graduand
Alberto Cercato
Matriculation Number 876808

Academic Year
2022 / 2023

Dedico questa tesi alla persona il cui desiderio più grande è conoscere, almeno in parte, la conoscenza che acquisiamo studiando l'universo. Guerra e povertà hanno distrutto questo sogno, ma è stato il coraggio che hai avuto a dare la possibilità alla tua famiglia di esaudirlo al tuo posto. Perciò, in quanto membro di suddetta famiglia, è ora il mio turno di dire: GRAZIE NINA.

CONTENTS

1 INTRODUCTION

Nowadays, the progressive increase in the global average temperature has emerged as the foremost consequence of climate change, posing a significant threat to sustainable development due to its impacts on the environment, economy, and society. Particularly, Tochaiwat et al. (2023) described the loss of thermal comfort for population of urban areas as major threat to society during summer, with direct and indirect effects on the economy and environment.

To date, efforts to combat excessive summer temperatures within cities have focused on downstream solutions, such as air conditioning systems, to cool indoor spaces within artificial structures. However, this choice proved to be unsustainable because of the significant economic and environmental costs. For example, the increased cooling energy consumption in summer season causes both a high economic expense for the purchase of electricity and a high environmental expense related to its production (Li et al., 2019). As a consequence, climate change becomes self-sustained, creating a dangerous loop that affects not only human beings but also all ecosystems and their processes. Moreover, focusing on ensuring comfort within facilities has not solved the problem of high temperatures for those who engage in outdoor activities, and summer heatwaves are still a major cause of public health resulting in high healthcare costs (Singh et al., 2020).

During the summer period, highly artificial areas experience a greater temperature increase compared to more natural areas, thus amplifying the increase in temperatures linked to climate change. This phenomenon is called Urban Heat Island (UHI) effect and highlights a temperature increase between 5 and 10°C (Heaviside et al., 2017) in urban area compared to surrounding rural areas, primarily due to the increasing of artificial elements and human activities (Mohajerani et al., 2017). Urbanization implies the replacement of natural and seminatural elements in favour of artificial ones. Artificial buildings and structures within cities absorb and retain heat from the sun, causing surfaces and local climate to become much hotter than in natural and seminatural elements. Indeed, artificial elements, composed by artificial material, do not provide a cooling effect just as the natural elements due to the presence of vegetation (Jacobs et al., 2020). At the same time, urbanization increases the intensity of several human activities that release heat. One of the most significant activities is air conditioning of buildings, which inherently generates a greater level of heat (Grimmond, 2007). Additionally, the contribution of other human activities on enhancing UHI effect was highlighted by the Covid-19's pandemic lockdown where, according to (Wai et al., 2022), in five international cities the UHI intensity has reduced.

Secondly, the wind blocking effect by buildings and the local release by human activities of heat and pollutant, as Greenhouse Gasses (GHGs) or particulate matter, also contribute to the UHI effect

(Singh et al., 2020). The reduction of wind within cities creates a more stagnant air more difficult to be mixed with cooler air from nearest areas through the convective heat transfer (Yan et al., 2022). Air mixing is also hindered by the high temperature itself that causes the instauration of local Hardley type of circulation that does not allows the dispersion of pollutants outside the urban area (Oke, 1974). In addition, pollutants that include GHGs and particulate matter absorb and hold part of infrared radiation emitted from the ground creating a local greenhouse effect. Moreover, high temperature increases photochemical smog production rate, enriching the air of more dangerous pollutants. Therefore, there exists a synergy between UHI and urban pollution island (Ulpiani, 2021) that further threats human health.

Additionally, the increase in temperature and the decrease in ventilation result in an increase in relative humidity that fosters the UHI effect reinforcing the loss of thermal comfort. As a result, the physiologically equivalent temperature (PET) further increases causing heat stress for humans (Fahed et al., 2020).

Recently, research highlighted the crucial role that natural land cover can play in supplying a cooling effect service in urban areas, thereby possibly representing an upstream solution able to ensure thermal comfort and sustainability simultaneously (Tochaiwat et al., 2023). Indeed, several studies emphasised the benefits for the economy and society given by cooling effect service related to natural and seminatural landscape elements, such as the protection of human health (Norton et al., 2015; Jay et al., 2021) or the reduction of energy consumption to lower temperature inside buildings (Elmqvist et al., 2015).

According to Su et al. (2022) the vegetation present in green landscape elements provides cooling effect essentially through canopy shading and evapotranspiration. Canopy shading induces the sheltering effect of sunlight. This phenomenon refers to the canopy's ability to protect the underlying ground from the direct sunlight, thereby reducing the ground adsorption of energy and lowering the ground temperature. The subsequent decrease in infrared radiation emissions from the ground in turns leads to a reduction of local temperature. Conversely, evapotranspiration, changing the state of water from liquid to gas, consumes the energy provided from the sunlight as latent heat of evaporation, thereby reducing sensible heat which is responsible for increasing ground temperature. In this way a decrease in ground temperature leads to a reduction in the emission of infrared radiation from the ground, reducing the local temperature.

Moreover, Sugawara & Takamura (2014) observed that the presence of vegetation in urban areas increases albedo, providing a brighter surface than artificial urban materials. Scientific research has already confirmed the existence of a negative relationship between albedo and local temperature

(Andrés-Anaya et al., 2021; Tahooni et al., 2023), because of the lower amount of energy absorbed by physical bodies within artificial areas.

It is also important to consider that vegetation, through the sequestration of CO_2 which primarily results is an increase of the average global temperature, has a strong capacity to mitigate climate change. Therefore, vegetation provides thermal comfort even in the long term on a global scale. Thus, limiting urbanization on a large scale with proper landscape management and the restoration of green elements in human dominated areas may be an effective way to restore the thermal comfort directly and indirectly through climate change mitigation (Shadman et al., 2022). Despite some recent literature questioned the contribution of urban vegetation to climate change mitigation through e.g., carbon stock (e.g., Velasco et al., 2016; Zhang et al., 2022), several studies are consistent in highlighting that confirmed it is indubitable that the removal and fragmentation of natural or seminatural landscape elements due to strong urbanization has led to the alteration of ecosystem processes and a decrease of the ecosystem services provided, including cooling effect (Weng et al., 2004; Zhang et al., 2022; Guo et al., 2015; Qiu et al., 2017).

To overcome the problem, the European Union is promoting policies for cities and rural areas in order to reintegrate natural elements to cope with climate change impacts and build sustainable and resilient cities. In particular, in 2013 the European Commission adopted an EU strategy on Green Infrastructure (GI strategy) (European Union, 2013). GI is defined as a network of natural and seminatural areas, as well as green spaces, strategically planned and managed to deliver a wide range of ecological, economic, and social benefits by providing multiple ecosystem services (European Union, 2013). GI is also mentioned in the new EU Strategy on Adaptation to Climate Change (European Union 2021) as a nature-based solution to adapt to climate change.

Several authors (Mell, 2009; Marando et al., 2022; Coutts & Hahn, 2015) have highlighted Green Infrastructure (GI) as one of the main measures to restore the supply of ecosystem services and the benefits for the population. However, despite the recognized role of GI, there still remains uncertainty as far as GI spatial structure and configuration are concerned as well as about the role these GI features play in providing ecological functions and supplying services. Retrieving insights about the composition and the spatial configuration of the patches within a GI to maximize Ecosystem Services (ESs) supply and the flow and understanding how they change across scales are crucial for ensure the sustainability of GI interventions (Heremans et al., 2021; Capotorti et al., 2023).

With reference to the enhancement of the cooling effect service, only a few studies analysed aspects related to composition and configuration attributes of landscape and patches to retrieve useful insights for GI implementation. For example, Chen et al. (2022) and Zhang (2020) have focused only on

aspect related to the composition of patches, while Kowe et al. (2021), Zhang et al. (2022) and Zhang et al. (2009) have focused on spatial configuration of GI's elements.

Additionally, the studies conducted till now have evaluated the influence of landscape and patch attributes only based on a unique scale investigation (i.e., local scale or regional scale). Thus, cross-scale evaluation of the influence of such attributes on ESs supply is still lacking and requires to be addressed (Li et al., 2023). Particularly, the evaluation of the influence of both composition and configuration attributes on ESs capacity and supply differences across scales is likely to provide useful insights to help the strategical planning of an effective Green Infrastructure (Lindborg et al. 2017).

Moreover, studies conducted to date focused mainly on metropolitan cities centres, i.e., areas with high population density, characterized by a compact and very homogeneous built-up area. Conversely, areas characterized by low-density population and buildings have mostly been neglected, precluding the study of cooling effect on all the continuum of variability for landscape and patch attributes necessary to fully understand the supply of this ES. Thus, the study on small cities typical of the countryside is an important opportunity to better understand the influences of the GI's composition and configuration attributes of green elements to cooling effect supply because of their major variability of green areas with respect to metropolitan city contexts.

In such a context, our aim is to clarify the effect of GI element attributes on the provision of the cooling effect and the thermal comfort to people and investigate the differences of ES supply for different natural and seminatural elements across scales and in different land use and land cover settings to define requirements and insights for a proper GI planning (Lindborg et al., 2017).

Specifically, we defined two main research questions at two different spatial scales: i) How is cooling effect related to landscape composition and configuration attributes of natural and seminatural areas? (Landscape level); ii) How does cooling effect vary according to patch type and configuration? (Patch level). A multiscale approach will allow a comprehensive evaluation of cooling effect.

1.1 Green Infrastructure

To foster the supply of a wide range of ecosystem services (ESs) in urban and rural areas, including cooling effect, the European Union implemented the Green Infrastructure Strategy (European Union, 2013). This policy instrument aims to implement a nature-based solution called Green Infrastructure (GI), which is an evolution of the concept of ecological network that operates in human dominated areas. GI aims at conserving biodiversity as a key element for the ESs supply useful to ensure

multibenefits purpose (Jones & Somper, 2014; Matthews et al., 2015; De la Sota et al., 2019). Basically, the spatial structure of GI, like any ecological network, consists of an array of corridors or stepping stones (link) that connect core areas (hub). Due to the intense exploitation of urban and rural areas, space represents the major constraint for ecosystems and the elements that compose links and hubs. GI elements can have both a vegetated and an artificial component (hybrid solutions), where other elements can be totally natural. However, GI elements aims at substituting some artificial elements serving the same function and additional secondary functions simultaneously, this property is called multifunctionality (European Union, 2012). Rain gardens (Fig. 1.1) well exemplify the concept of multifunctionality. Here, substrate (that can be natural or artificial) and plant roots promote water infiltration, while vegetation also provides other services such as cooling effect, pollination, aesthetic beauty, and more. Other examples of GI elements are recreational green areas, tree lines, green walls, bioswale, rooftop gardens, tree box filters, and green traffic islands (Fig. 1.1).

Figure 1.1: a) bioswale (source: Living concept, 2013, https://www.livingconceptslandscape.com/2015/09/bioswales/), b) green traffic island (source: Sempergreen, https://www.sempergreen.com/en/references/traffic-island), c) green wall (source: Tiziona Codiferro, https://www.codiferro.it/la-fertirrigazione-come-nutrire-le-piante-attraverso-lirrigazione/), d) rain garden (source: Paul Edwars, https://www.pinterest.it/pin/306315212140896953/), e) rooftop garden (source: Instapro, https://www.instapro.it/porte-finestre/articoli/pac-s19-vantaggi-svantaggi-tetto-verde), f) tree box filter (source: flickr, https://www.flickr.com/photos/mocobio/8816807664), g) tree line (source: bikewinnipeg, 2016, https://www.bikewinnipeg.ca/event/webinar-planning-for-facility-maintenance-and-management-costs/), h) recreational green area (source: u-earth, https://it.u-earth.eu/smart-cities)..

Strategic landscape planning is needed to ensure the effectiveness and the multifunctionality of GI and go further the constitution of single separate green elements of urban and rural areas. Indeed, the primary aim of strategic GI planning is to develop structural connectivity, and consequently, the species-specific functional connectivity. Functional connectivity represents the base to sustain biodiversity and ecosystem processes (Salomaa et al., 2017). From an ecological perspective, GI is crucial for the conservation of those ecological functions that underpin ESs provision, maintaining the diversity of ESs provided and, consequently, the multifunctionality of a GI according to Harrison

et al. (2014). Soulé et al. (2004) suggested that ecological connectivity should be preserved and investigated at different spatial scales to optimize biodiversity conservation. Thus, to increase the resilience of the GI networks, it is important to involve landscape planning at different spatial scales: neighborhood, district, urban settlement, municipality, province, region, etc.

From a social and economic point of view, strategic GI planning has strong benefits for the sustainable development of urban and rural areas. A properly planned GI optimizes both the supply and the flow of ESs, avoiding conflicts of interest that may arise from law, security, available space, and available founding. For example, a correct planning to implement a GI able to provide noise reduction service, so strategically locating green elements in a site with significant noise pollution, such as the border of a road or a railroad, allows the coexistence of economic and social activities in the same place.

2 MATERIALS AND METHODS

2.1 Study area

The study took place in the Cartigliano Municipality, located in northeastern Italy, in the Veneto Region (45° 42´ 26.950" N, 11° 42´ 0.436" E) (Fig. 2.1).

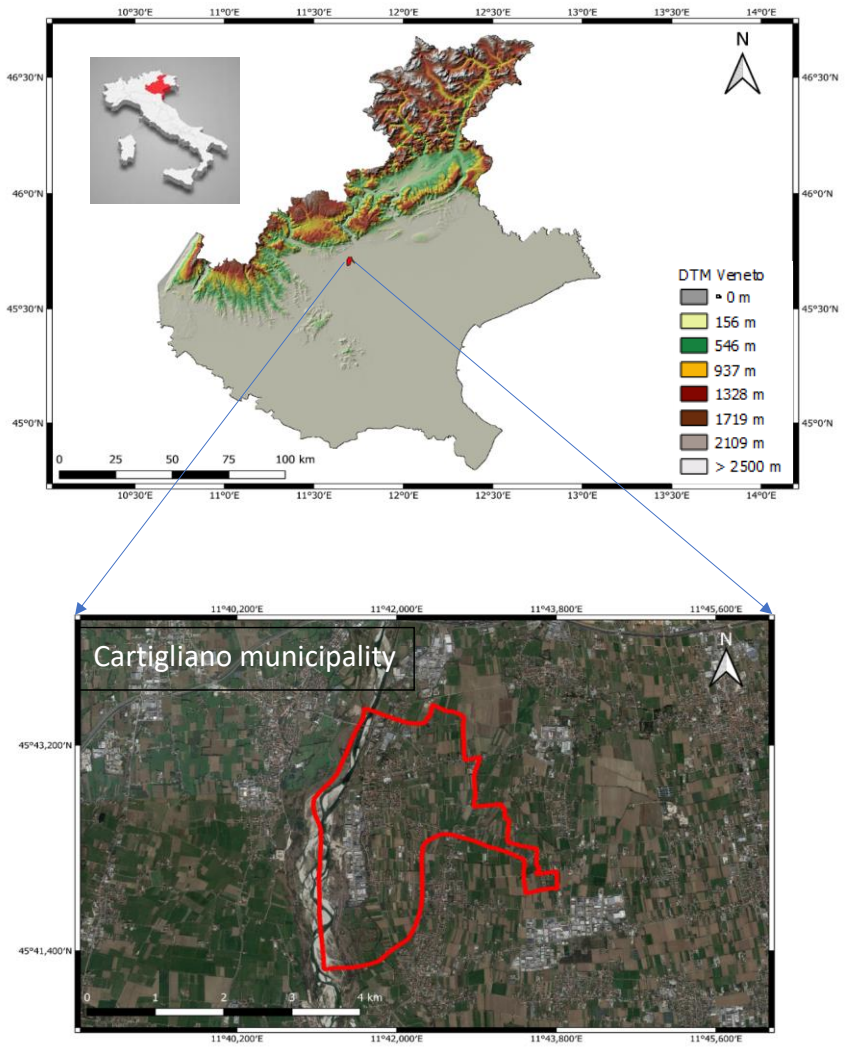

Figure 2.1: Location of the study area

In 2021, the municipality counted 3711 residents (ISTAT https://www.tuttitalia.it/veneto/95-cartigliano/statistiche/popolazione-andamento-demografico/) for an area of approximately 7.37 km^2. Most of the territory of Cartigliano is characterized by the presence of agricultural land (48%), followed by natural areas (linked to SIC/ZPS "Grave e zone umide della Brenta" IT3260018; 24%), residential areas (22%), and industrial areas (6%; Fig. 2.2).

Field Code Changed

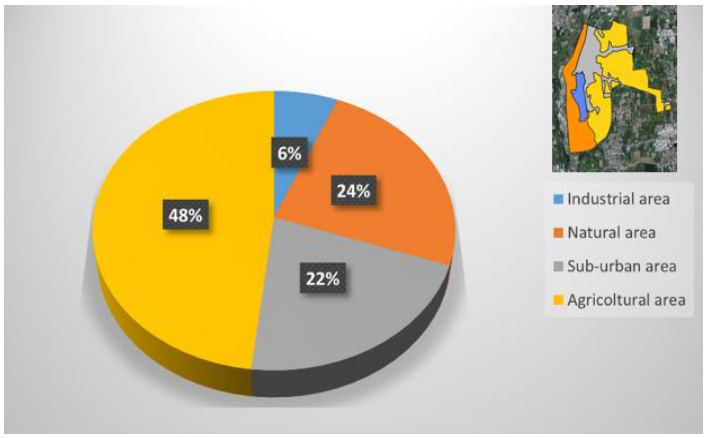

Figure 2.2: Land use and land cover repartition of Cartigliano municipality surface

Based on ARPAV database (https://www.arpa.veneto.it/dati-ambientali/open-data/) which provides measurements from 1994 to 2022 carried out by the station located in the nearby municipality of Rosà (Annex 1), the mean maximum air daily temperature is 28.1°C for June, 30.3°C for July, and 30°C for August, while the mean air temperature is 23.4°C for June, 24°C for July, and 23.8°C for August (Fig. 2.3). The precipitation regime is bimodal with a lower maximum in spring and a higher maximum in autumn (Bocchiola et al., 2013; Fig. 2.3).

Field Code Changed

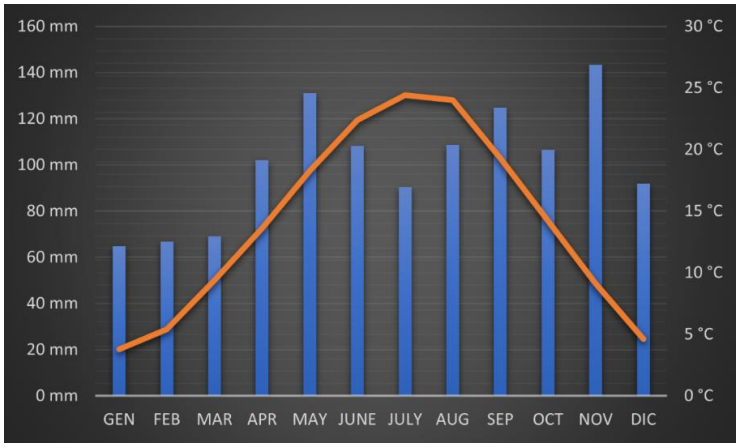

Figure 2.3: Climogram obtained from the ARPAV Rosà station mesurements. The colums show the variation of the mean monthly rainfall, the line shows the variation of the mean monthly air temperature.

Wind speed (ARPAV database; https://www.arpa.veneto.it/dati-ambientali/open-data/) varies from 0.6 m/s in June to 0.4 m/s in July and August, indicating low wind condition during summer, a feature typical of Po Valley climate (Bocchiola et al., 2013).

Field Code Changed

2.2 Mapping Land Use and Land Cover of the study area

To quantify patch and landscape attributes, we constructed a categorical map at 1m of resolution. Through QGIS 3.22.6 and GuidosToolbox software, we first processed AGEA 2018 orthophotos of the study area (available at https://idt2.regione.veneto.it/). Through the segmentation process based on the information associated to each pixel, we retrieved a vector layer output in which patches corresponded to different landscape elements. Due to the presence of shadows, it was necessary to edit the vector layer to correct patches boundaries across the entire surface of the Cartigliano municipality. Additionally, another correction was required to address the presence of small micro-polygons generated by the GuidosToolbox software (<0.001 m^2). To merge micro-polygons to the closest polygon that shared more perimeter, we used the "multiparts to singleparts" function.

Field Code Changed

After completing the correction for the vector layer, we classified each patch according to EUNIS classification system (version 2021; https://eunis.eea.europa.eu/habitats.jsp) using the third level of classification resolution. Once the categorical map was obtained, we updated and validated the map through field inspections in the study area.

Field Code Changed

2.3 Mapping Land Surface Temperature of the study area

Following Goldblatt et al. (2021), Land Surface Temperature (LST) was used as a proxy of air temperature, and thus, thermal comfort. According to Copernicus Global Land Service geoportal (https://land.copernicus.eu/global/products/LST), LST represents the radiative skin temperature of the land surface, as measured in the direction of the remote sensor.

Field Code Changed

2.3.1 Landscape level LST: 30x30m LST images

To investigate cooling effect at landscape level, Landsat 8 C1-Level 2 satellite images at 30 m of resolution were downloaded from U.S. Geological Survey (USGS) GloVis (https://glovis.usgs.gov/app). We considered data available for the last five years (from 2018 to 2022).

Field Code Changed

To ensure proper quality of data, we only selected dates that met specific requirements. Particularly, we selected images acquired during the summer season (between 15th May and 15th September) which exhibited no clouds or cloud shadows over the study area, and no rainfall events (minimum 1mm/h) up to two days before the acquisition date. While clouds can directly alter image quality, rain can influence the LST through evaporations (Sun et al., 2016). Thus, a total of nine images were selected, i.e., 30th June 2018, 17th August 2018, 1st June 2019, 17th June 2019, 19th July 2019, 5th September 2019, 22nd August 2020, 25th August 2020, and 10th September 2021.

LST was calculated for each selected images according to Stathopoulou & Cartalis (2007) as summarized in Fig. 2.4.

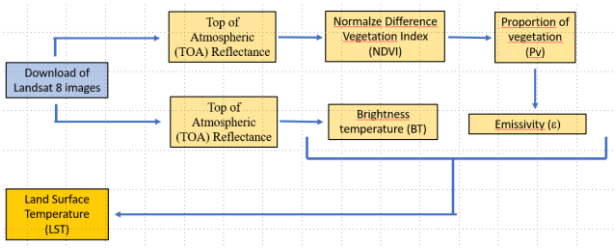

Figure 2.4: Method to obtain LST maps at a resolution of 30x30m

We first processed in GIS environment each Landsat 8 image to compute the Normalize Difference Vegetation Index (NDVI) through the following formula (Tucker, 1979):

$$NDVI = \frac{NIR - Red}{NIR + Red} \quad (2.1)$$

where:

- *NDVI* = Normalize Difference Vegetation Index;
- *NIR* = TOA Reflectance of band 5 (watts m^{-2} $srad^{-1}$ μm^{-1});
- *Red* = TOA Reflectance of band 4 (watts m^{-2} $srad^{-1}$ μm^{-1}).

Once created NDVI maps, we calculated the Proportion of Vegetation (Pv) using the following formula (Yu et al., 2014; Al-Shaar et al., 2022):

$$Pv = \left(\frac{NDVI - NDVImin}{NDVImax - NDVImin}\right)^2 \quad (2.2)$$

where:

- *NDVI* = Normalize Difference Vegetation Index;
- *NDVImin* = minimum Normalize Difference Vegetation Index;
- *NDVImax* = maximum Normalize Difference Vegetation Index.

Through Pv maps, we then calculated land surface Emissivity (ε). To compute Emissivity (ε), we followed the threshold method proposed by Sobrino et al. (2004). Specifically, the method suggests attributing a ε value of 0.97 for every pixel with a NDVI < 0.2 and a ε value of 0.99 for every pixel with a NDVI > 0.5. Instead, for pixels with a NDVI ≥ 0.2 and ≤ 0.5, the ε value must be computed using the following formula:

$$\varepsilon = 0.004 * Pv + 0.986 \quad (2.3)$$

where:

- ε = Emissivity;
- Pv = Proportion of vegetation.

Simultaneously, we computed the Brightness Temperature (BT). The computation of BT needed first the conversion of the Digital Numbers (DNs) to Top of Atmospheric (TOA) Reflectance for band 10 of Landsat 8 images, using the following formula (Al-Shaar et al., 2022):

$$TOA\ (L) = ML * Qcal + AL \quad (2.4)$$

where:

- TOA (L) = Top of Atmospheric Reflectance for band 10 (watts m^{-2} $srad^{-1}$ μm^{-1}).

- ML = band-specific multiplicative rescaling factor from the metadata for band 10 (RADIANCE_MULT_BAND_10 = 0.000342);
- Qcal = value of the band 10 satellite image;
- AL = band-specific addicting rescaling factor from the metadata for band 10 (RADIANCE_ADD_BAND_10).

Thereafter, we computed the BT as follow (Kowe et al., 2021; Al-Shaar et al., 2022):

$$BT = \frac{K2}{\ln\left[\left(\frac{K1}{L}\right)+1\right]} - 273.15 \quad (2.5)$$

where:

- BT = Brightness temperature (C°);
- K2 = band-specific thermal conversion constant from the metadata for band 10 (K2_COSTANT_BAND_10 = 1321.0789);
- K1 = band-specific thermal conversion constant from the metadata for band 10 (K1_COSTANT_BAND_10 = 774.8853);
- L = TOA Reflectance for band 10 (watts m^{-2} $srad^{-1}$ μm^{-1}).

The ε and the BT maps were then used to create the LST maps for the whole study area using the following formula (Al-Shaar et al., 2022):

$$LST = BT/(1 + \left(0.00115 * \frac{BT}{1.4388}\right) * \ln(\varepsilon))) \quad (2.6)$$

where:

- LST = Land Surface Temperature (°C);
- BT = Brightness temperature (°C);
- ε = emissivity.

At the end of the process, we averaged the values of the nine LST raster images in GIS environment to define a unique summarizing LST image (30 meters of resolution) for summer temperatures.

2.3.2 Patch level LST: 3x3m LST images

To investigate the cooling effect at patch level, we obtained LST maps at higher resolution (3m) by processing Landsat 8 images following Kowe et al. (2021), and combining PlanetScope satellite images, as summarized in Fig. 2.5. Particularly, we used PlanetScope satellite images to retrieve Emissivity (ε) at a finer scale and calculate LST as in formula (2.6).

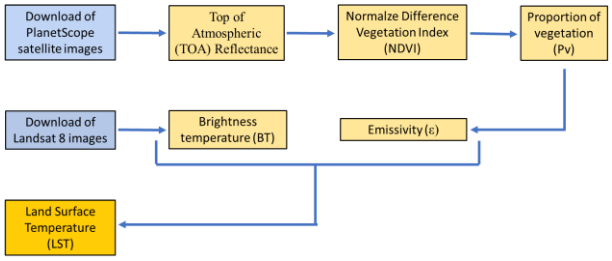

Figure 2.5: Used method to obtain LST maps at a resolution of 3x3m

PlanetScope surface reflectance satellite images with thermal bands were downloaded for the each of the nine dates considered for the LST at 30m resolution (source: https://www.planet.com/). To correct the reflectance of the atmosphere, we considered coefficient indicated on metadata (Annex 2) and considered the proper bands useful to retrieve all data necessary to compute ε. To convert the Digital Numbers (DNs) to Top of Atmospheric (TOA), we selected reflectance for band 3 (Red) and 4 (NIR) for each downloaded images using the following formula in GIS environment:

Field Code Changed

$$TOA = DNs * k \quad (2.7)$$

Where:

- *TOA* = Top of Atmospheric Reflectance (watts m^{-2} $srad^{-1}$ μm^{-1});
- *DNs* = Digital numbers;
- *k* = Reflectance coefficient specific for the band considered and the condition of atmosphere at the time of the shooting (Annex 2).

We then used the corrected bands to calculate NDVI as in Tucker (1979), that is:

$$NDVI = \frac{NIR - Red}{NIR + Red} \quad (2.8)$$

where:

- *NDVI* = Normalize Difference Vegetation Index;
- *NIR* = TOA Reflectance of band 4 (watts m^{-2} $srad^{-1}$ μm^{-1});

- *Red* = TOA Reflectance of band 3 (watts m^{-2} $srad^{-1}$ μm^{-1}).

Next, we created Pv and ε maps using the finer NDVI map values in the before mentioned formulas (i.e., 2.2, 2.3 respectively). As a result, we obtained nine emissivity maps at 3m resolution to be used in the LST calculation.

To align the resolution of BT and ε, we performed the "cubic spline" interpolation for the sharpening of each of the previous nine 30x30 m BT maps according to Maeland (1988) and Aslam et al. (2016). As a result, we obtained 3m resolution BT maps and we computed LST at 3m resolution using the beforementioned formula (2.6) by considering both ε and BT performed at 3m of resolution.

At the end of the process, we averaged the values of the nine LST raster images in GIS environment to define a unique summarizing LST image (3 meters of resolution) for summer temperatures.

2.4 Data collection for cooling effect quantification

Land surface temperature was used to address the influence of composition and configuration attributes on cooling effect at two different spatial scales.

At landscape level, analyses aimed to:

- ia) investigate the relationship between LST of built areas with no vegetation (non-vegetated patches; Tab 2.1) and landscape composition and configuration attributes of green areas (i.e., all vegetated patches in the study area; Tab. 2.1), namely number and total area of green patches.
- ib) investigate the relationship between LST of non-vegetated patches and attributes of green areas divided into two subcategories, namely "herbaceous patches" and "woody patches". Herbaceous patches included all landscape categories characterized by herbaceous communities, while woody patches included all landscape categories related to woody vegetation communities (Tab. 2.1). Thus, we considered composition and configuration attributes at landscape level, i.e., number and total area for both herbaceous and woody patches.
- ic) investigate the relationship between LST of non-vegetated patches and the ratio between total woody area and total herbaceous area.

At patch level, analyses aimed to:

- iia) investigate which type of vegetated patches between highly managed herbaceous communities of suburban and industrial areas (urban green areas), seminatural grasslands and hedgerows (Tab. 2.2) provide the highest capacity for cooling effect.

- iib) investigate the relationship between LST of urban green areas, hedgerows, and grasslands patches, and patch configuration attributes as area, perimeter, and shape.

2.4.1 Cooling effect at Landscape level

To investigate cooling effect at landscape level, we grouped the EUNIS classes as in Tab. 2.1 to account for the effect of vegetated areas (Macro-category) and of green area types (Sub-category) on LST of non-vegetated areas. To this aim, a 300x300m grid was created within the Cartigliano Municipality (Fig. 2.6). Since QGIS operators did not work for partly empty cells, we only considered completely full cells (n= 55), avoiding cells along the municipal boundaries.

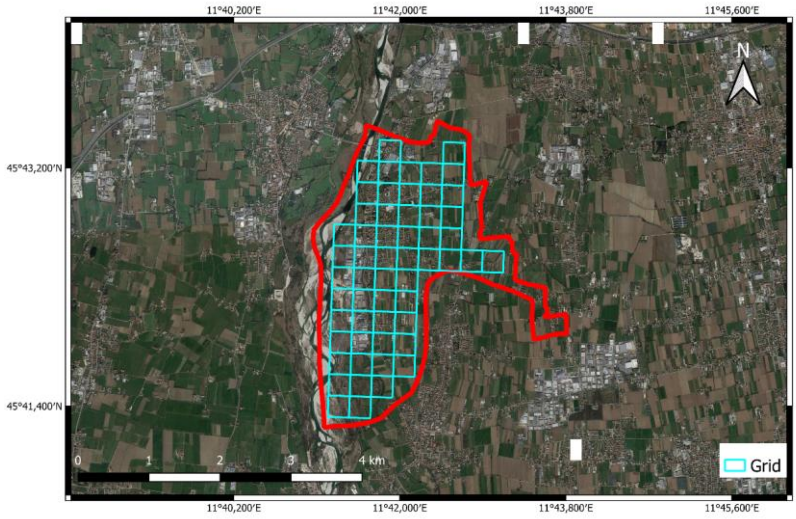

Figure 2.6: Grid within Cartigliano municipality

Afterwards, we created a simplified categorical map, by assigning each polygon within a 300x300m cell to a macro-category as reported in Tab. 2.1. Moreover, within the "green areas" category we further identified two sub-categories, namely "herbaceous patches" and "woody patches" to account for the green area type, considering the complexity of the structure (number of different strata) of plant communities (Tab. 2.1). As a result, we associated two new attributes to each patch in the categorical map: one for the macro-category (value 0 = non-vegetated area, value 1 = green area), and the second to distinguish the sub-category (green area type) within green area (value 0 = non-vegetated area, value 1 = herbaceous patch, value 2 = woody patch).

Table 2.1 EUNIS categories found in the study area, grouped into macro-categories and sub-categories.

Macro-category	Sub-category	EUNIS code	Description
Built areas/non-vegetated areas		C36	Unvegetated or sparsely vegetated shores with soft or mobile sediments
		J11	Residential buildings of city and town centres
		J12	Residential buildings of villages and urban peripheries
		J13	Urban and suburban public buildings
		J14	Urban and suburban industrial and commercial sites still in active use
		J15	Disused constructions of cities, towns and villages
		J16	Urban and suburban construction and demolition sites
		J21	Scattered residential buildings
		J22	Rural public buildings
		J23	Rural industrial and commercial sites still in active use
		J24	Agricultural constructions
		J25	Constructed boundaries
		J26	Disused rural constructions
		J27	Rural construction and demolition sites
		J32	Active opencast mineral extraction sites, including quarries
		J33	Recently abandoned above-ground spaces of extractive industrial sites
		J41	Disused road, rail and other constructed hard-surfaced areas
		J42	Road networks
		J46	Pavements and recreation areas
		J47	Constructed parts of cemeteries
		J61	Waste resulting from building construction or demolition
		J62	Household waste and landfill sites
		J64	Agricultural and horticultural waste
		J65	Industrial waste

Green areas	herbaceous	C32	Water-fringing reedbeds and tall helophytes other than canes
		C35	Periodically inundated shores with pioneer and ephemeral vegetation
		R1A	Semi-dry perennial calcareous grassland (meadow steppe)
		R22	Low and medium altitude hay meadow
		V11	Intensive unmixed crops
		V12	Mixed crops of market gardens and horticulture
		V13	Arable land with unmixed crops grown by low-intensity agricultural methods
		V15	Bare tilled, fallow or recently abandoned arable land
		V21	Large-scale ornamental garden areas
		V22	Small-scale ornamental and domestic garden areas
		V23	Recently abandoned garden areas
		V31	Agriculturally-improved, re-seeded and heavily fertilised grassland, including sports fields and grass lawns
		V38	Dry perennial anthropogenic herbaceous vegetation
		X07	Intensively-farmed crops interspersed with strips of natural and/or seminatural vegetation
		X22	Small city centre non-domestic gardens
	woody	S91	Temperate riparian scrub
		T11	Temperate Salix and Populus riparian forest
		T13	Temperate hardwood riparian forest
		V41	Hedgerows of non-native species
		V42	Highly managed hedgerows of native species
		V43	Species-rich hedgerows of native species
		V44	Species-poor hedgerows of native species
		V54	Vineyards
		V61	Broadleaved fruit and nut tree orchards
		V62	Evergreen orchards and groves
		V63	Lines of planted trees

To evaluate the effects of green areas and green areas type on the temperatures of non-vegetated areas (i.e., non-vegetated areas), we first calculated the mean LST of non-vegetated areas (LST_{ART}) through "zonal statistic" function to sample the LST image (30m resolution) in each of the 55 cells. Then, for each cell we computed landscape composition and configuration attributes for green areas, namely the total area (TA_{GREEN}) and the number of patches (NP_{GREEN}). After rasterizing the vectorial map based on binary values (i.e., 0 – non-vegetated and 1 – green) at 1m resolution, we extracted the 55 rasterized cells of the grid using the "clip raster by mask layer" tool in QGIS and we uploaded them on Fragstats 4.2 (McGarigal et. Al, 1995) to perform a batch calculation of the selected attributes.

To explore the cooling effects of the two defined green types (i.e., herbaceous or woody communities) on LST of non-vegetated areas (LST_{ART}), we calculated the same attributes of the green areas for the two green types. In this case, we rasterized the vectorial map of the study area considering the sub-categories: 0 (non-vegetated area), 1 (herbaceous patches), and 2 (woody patches).

Then, we clipped the 55 rasterized cells of the grid using the "clip raster by mask layer" tool in QGIS and we uploaded them on Fragstats 4.2 (McGarigal et. al., 1995) to perform a batch calculation of the selected attributes for both sub-categories. Thus, we calculated the total area (TA_{HERB}) and the number of patches (NP_{HERB}) for herbaceous patches and the total area (TA_{ARB}) and the number of patches (NP_{ARB}) for woody patches for each cell.

Finally, to evaluate the combined effect of the two considered green types on the LST of non-vegetated areas (LST_{ART}), we considered the ratio between woody and herbaceous total areas (TA_{ARB}/TA_{HERB}) for each grid cell.

2.4.2 Cooling effect at Patch level

To investigate the cooling effect at the patch level, we randomly selected patches considering three different land cover classes, i.e., 100 urban green areas (URB), 100 hedgerows (HED), and 100 seminatural grasslands (GRA; Tab. 2.2). Specifically, we conducted random selection of patches across the entire municipal territory in order to ensure proper variability in terms of patch configuration attributes (i.e., area, perimeter and shape) necessary to explore their contribution on cooling effect.

Table 2.2 EUNIS categories repartition to urban green areas, hedgerows and grasslands.

Macro-category	EUNIS code	Description
	V21	Large-scale ornamental garden areas

Urban green areas	X22	Small city centre non-domestic gardens
Hedgerows	S91	Temperate riparian scrub
	T11	Temperate Salix and Populus riparian forest
	T13	Temperate hardwood riparian forest
	V41	Hedgerows of non-native species
	V42	Highly managed hedgerows of native species
	V43	Species-rich hedgerows of native species
	V44	Species-poor hedgerows of native species
Grasslands	V31	Agriculturally-improved, re-seeded and heavily fertilised grassland, including sports fields and grass lawns
	V38	Dry perennial anthropogenic herbaceous vegetation

To quantify the cooling effect, we figured out the mean LST for each patch of urban green areas (LST_{URB}), hedgerows (LST_{HED}), and grasslands (LST_{GRA}), through the application of "zonal statistic" tool in QGIS on the 3 meters of resolution LST images.

In addition, for each selected patch we calculated the following configuration attributes using field calculator of QGIS: area, perimeter, and shape index. Namely, we calculated $AREA_{URB}$, $PERIMETER_{URB}$, and $SHAPE_{URB}$ for urban green area patches; $AREA_{HED}$, $PERIMETER_{HED}$, and $SHAPE_{HED}$ for hedgerows patches; $AREA_{GRA}$, $PERIMETER_{GRA}$, and $SHAPE_{GRA}$ for seminatural grasslands patches. While area and perimeter were directly computed by QGIS commands, we used the following formula to calculate the shape index (McGarigal et al., 1995):

$$SHAPE = \frac{pij}{2 * \sqrt{\pi * aij}} \quad (2.9)$$

where:

- pij = perimeter (m) of patch ij
- aij = area (m^2) of patch ij.

A shape index = 1 indicates a circular (regular) patch shape, while a SHAPE index value > 1 indicates non-circular (irregular) patch shape.

2.5 Data analysis

All data were uploaded in R software (version 4.2.1) to conduct statistical analyses.

2.5.1 Landscape data analysis

Before each analysis we constructed the Q-Q plot (Kovacevic, 2000) of the dependent variable to determine whether data were normally distributed and determine which statistical analysis to conduct. To perform analyses, we considered the LST of non-vegetated areas (LST_{ART}) of each of the 55 cells of the grid. Since the response variable LST_{ART} was found to be normally distributed (Fig. 2.7), we conducted parametric tests to investigate the first research question.

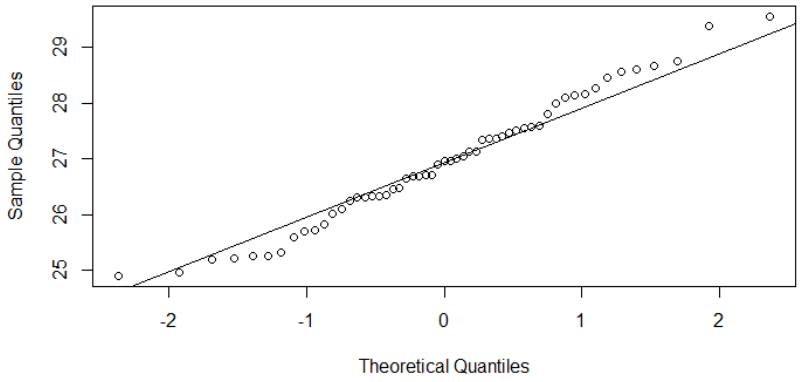

Fig. 2.7 Q-Q plot of LST_{ART}

Influence of green areas attributes on LST_{ART}

To assess the relationship between attributes of green areas and LST_{ART} at landscape level, we performed a linear regression model, lm() function in R (Kowe et al., 2021). Specifically, we investigated the relationship between LST_{ART} (response variable) and NP_{GREEN} and TA_{GREEN} (explanatory variables). Then, we defined the significance of the relationship and the variables that were significantly related to LST_{ART} considering a significance level (α) of 5%.

Influence of herbaceous and woody areas attributes on LST_{ART}

To investigate the relationship between attributes of green types, namely herbaceous and woody patches, and LST_{ART} at landscape level, we performed two linear regression models, lm() function in R: one for herbaceous patches and one for woody patches. In this case, we assessed the relationship between LST_{ART} (response variable) and NP_{HERB}, TA_{HERB} (explanatory variables) for herbaceous class, and the relationship between LST_{ART} (response variable) and NP_{ARB}, TA_{ARB} (explanatory

variables) for woody class. Thereafter, we defined the significance of the relationship and the variables that were significatively related to LST_{ART} by considering a significance level (α) of 5%.

Influence of woody and herbaceous total area ratio on LST_{ART}

To assess the relationship between the ratio of the two green types, namely the ratio between woody and herbaceous total areas, and LST_{ART}, we conducted a linear regression model, lm() function in R. Particularly, we considered the relationship between LST_{ART} (response variable) and TA_{ARB}/TA_{HERB} (explanatory variable). To define the significance of the relationship, we considered a significance level (α) of 5%.

2.5.2 Patch data analysis

As in the previous analysis, we first constructed the Q-Q plot (Kovacevic, 2000) of the dependent variables to determine whether data were normally distributed and determine which statistical analysis to conduct. Since the LST data showed to be normally distributed for each considered land cover class (Figs. 2.8, 2.9, 2.10), we conducted parametric tests for the analyses also to address the second research question.

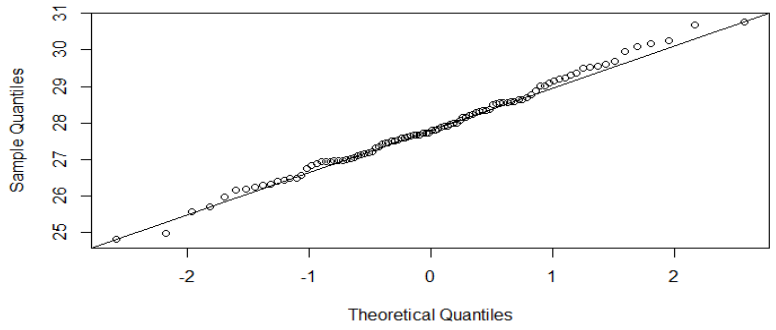

Fig. 2.8 Q-Q plot of LST_{URB}

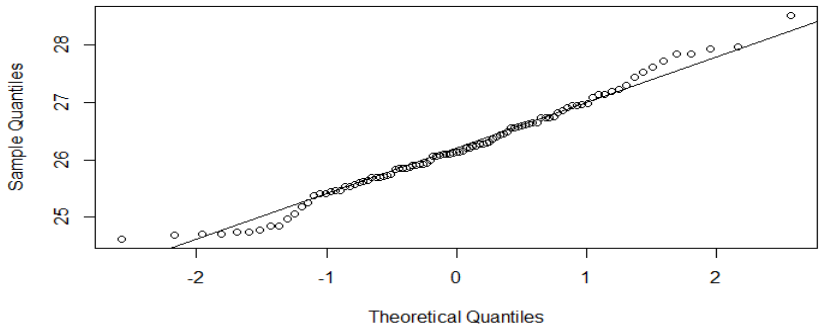

Fig. 2.9 Q-Q plot of LST_{HED}

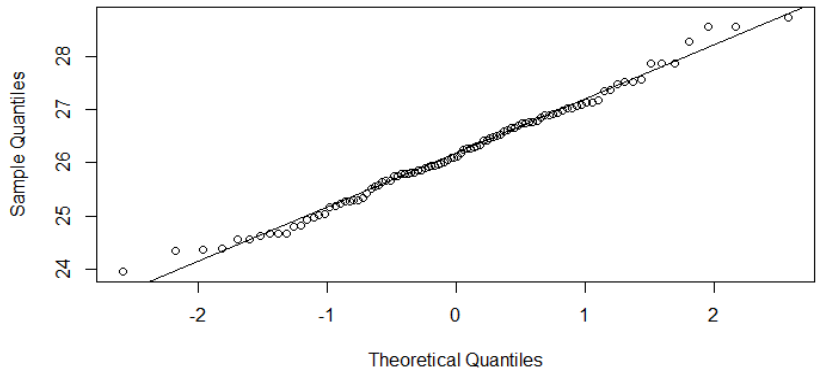

Fig. 2.10 Q-Q plot of LST_{GRA}

Urban green areas, hedgerows, and grassland mean LST

To assess whether urban green areas, seminatural grasslands and hedgerows significantly differed in terms of cooling effect capacity (LST_{URB}, LST_{HED}, LST_{GRA}), we performed the analysis of variance, aov(), considering a significance level (α) of 5%. Since the ANOVA test does not specify differences among groups (Abdi & Williams, 2010), we conducted a post-hoc Tukey's Honest Significant Difference (TukeyHSD) to do all pair wise comparisons and gain further information about the differences (Nanda et al., 2021).

Influence of urban green areas, hedgerows, and grasslands attributes to their LST

To detect dependences of cooling effect on patch configuration attributes, we performed a regression model for each green area type, lm(). For each type, we considered the relationship between LST (response variable) and area, perimeter and shape index (explanatory variables). Through backward selection, we selected those variables that were significantly related to LST, considering a significance level (α) of 5%.

3 RESULTS

3.1 EUNIS categorical map

The high-resolution map (Fig. 3.1) showed a total of 52 EUNIS III level categories within the Cartigliano Municipality, for a total of 8,238 patches (Annex 3).

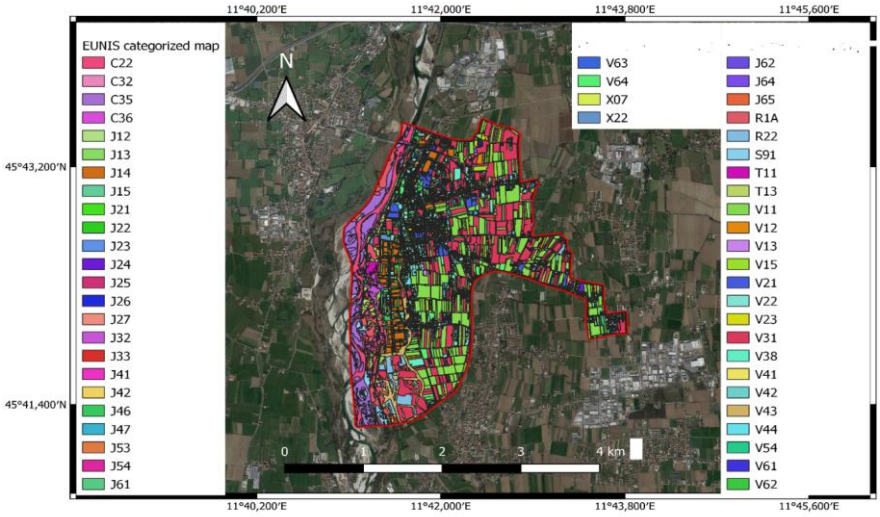

Figure 3.1: EUNIS categorical map of the study area.

3.2 Land Surface Temperature maps

Figure 3.2 shows the LST map at 30 meters of resolution obtained by averaging the nine selected LST images corresponding to the selected dates. The mean LST across the entire municipality of Cartigliano results of 25.41 ± 1.32 °C.

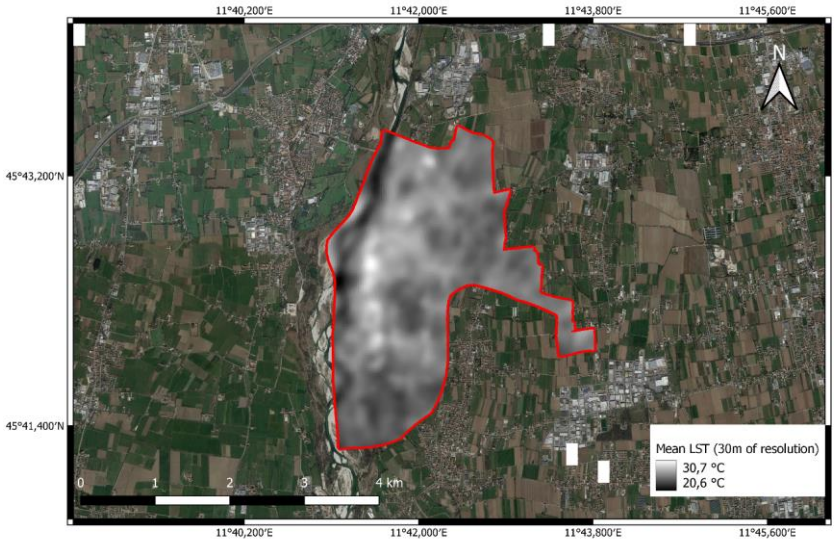

Figure 3.2: Map of LST at 30 meters of resolution.

Figure 3.3 shows the LST map at higher resolution (3m). Overall, the mean LST of Cartigliano results of 26.7 ± 1.45 °C.

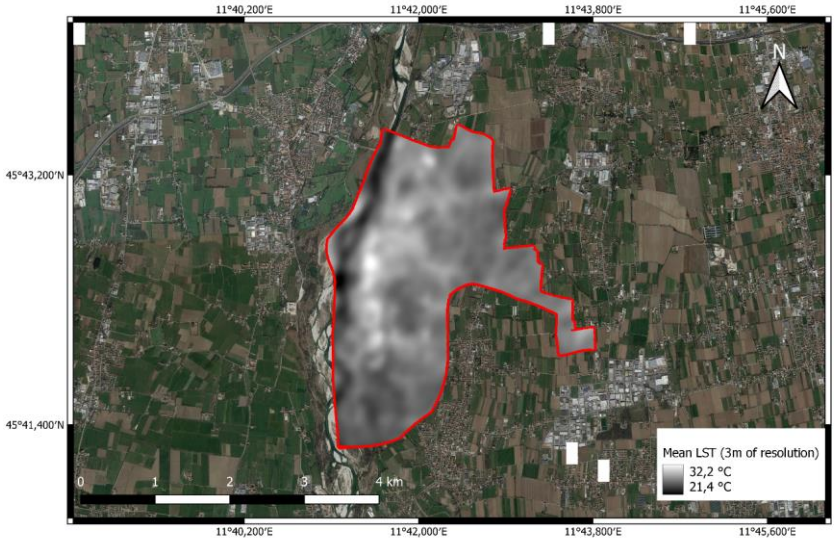

Figure 3.3: Map of LST at 3 meters of resolution.

3.3 Cooling effect at landscape level

Within the 55 cells under investigation, the mean cover of green areas (TA_{GREEN}) was 6.73 ± 1.8 ha while the mean number of green area patches (NP_{GREEN}) was of 25 ± 22.65. The distribution of green areas across the municipal territory was uneven, as illustrated in Fig. 3.4.

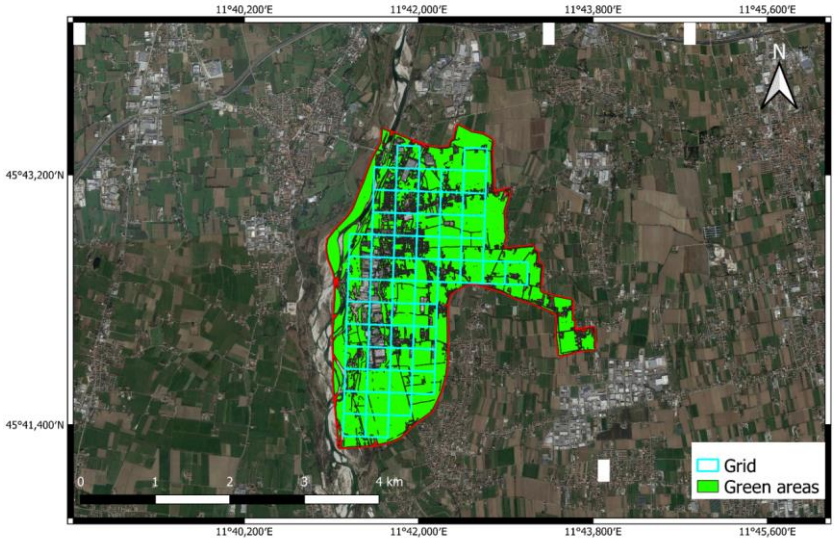

Figure 3.4: Green areas within the study area and the grid cells..

The distinction between herbaceous and woody vegetation communities within green areas of the municipal territory produced the maps shown in Fig. 3.5 and Fig. 3.6, respectively. The mean cover of herbaceous patches (TA_{HERB}) was of 5.31 ± 1.97 ha while the mean number of herbaceous patches (NP_{HERB}) was 27 ± 21.44; both the mean cover of woody patches (TA_{ARB}; 1.42 ± 0.8 ha) and their mean number (NP_{ARB}; 20 ± 20.95) were lower.

The mean and standard deviation values of green area and green type attributes across the 55 identified cells, confirmed the necessary variability we searched for the explanatory variables under analysis.

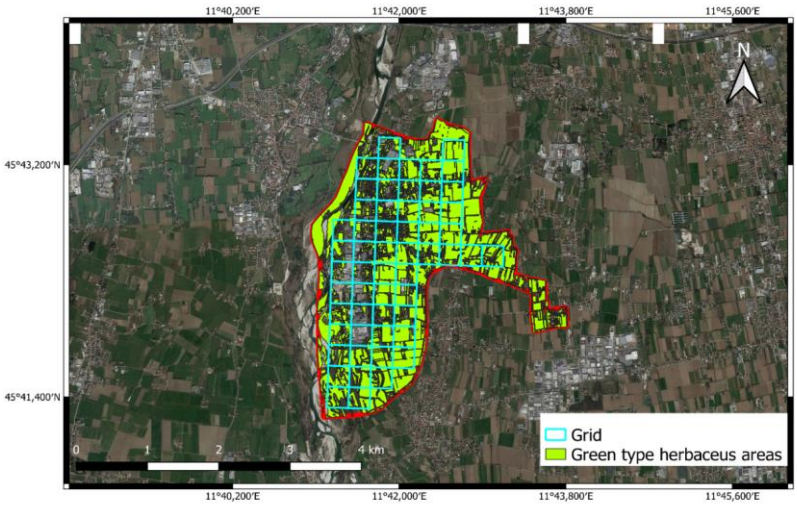

Figure 3.5: Herbaceus green areas within the study area and the grid cells.

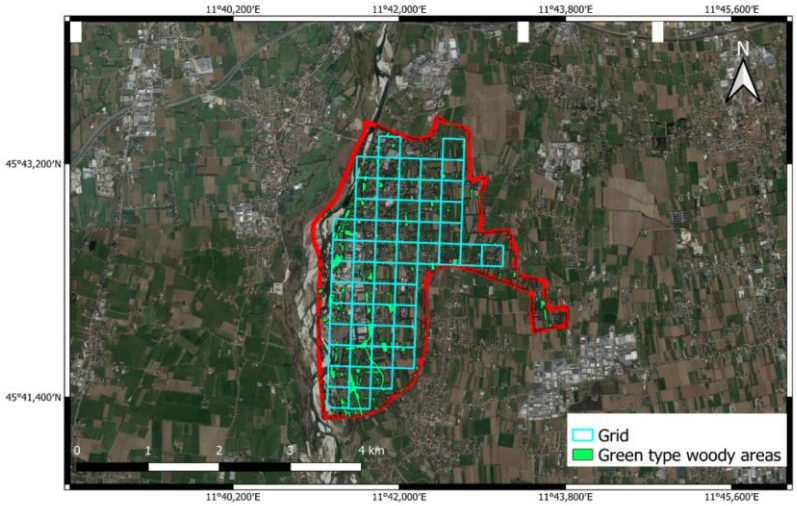

Figure 3.6: Woody green areas within the study area and the grid cells.

The mean LST of non-vegetated areas (LST_{ART}) within the 55 cells defined within the municipal territory, resulted of 26.94 ± 1.13 °C.

Influence of green area attributes on LST_{ART}

The regression model highlighted a significant relationship between LST_{ART} and the predictors (P-value: $1.663x10^{-12}$; Fig. 3.7). Particularly, we found a significant negative relationship between TA_{GREEN} and LST_{ART} (Tab. 3.1), meaning that lower values of LST_{ART} were related to higher values of green cover at the landscape level. Moreover, we found a significant positive relationship when considering the combined effect of TA_{GREEN} and NP_{GREEN} on LST_{ART} (Tab. 3.1). The last result suggests that there was a significant interaction between the two predictor variables influencing the response variable. Specifically, the significant positive estimate coefficient indicates that the two predictors affect LST_{ART} by changing in the same way. This means that lower LST_{ART} were reached for higher values of both TA_{GREEN} and NP_{GREEN}.

Tab. 3.1: statistical parameters of regression model between LST_{ART} and green area attributes.

Predictor	Estimated coefficient	Standard error	t-value	p-value
~ TA_{GREEN}	-0.559	0.102	-5.482	**$1.31x10^{-6}$**
~ NP_{GREEN}	-0.031	0.019	-1.641	0.107
~ TA_{GREEN}:NP_{GREEN}	0.007	0.003	2.316	**0.025**

Limit of significance: p-value < 0.05

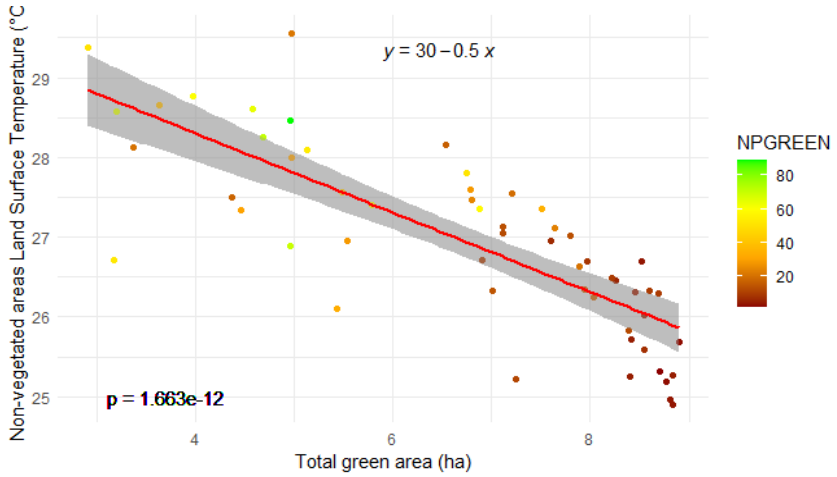

Figure 3.7: relathionship between LST_{ART} and the predictor variable TA_{GREEN} (identifiable throught the abscissas line), NP_{GREEN} (identifiable throught the colour gradient of the points), and TA_{GREEN}*NP_{GREEN} (identifiable trought the confidence band of the interaction).

Influence of herbaceous and woody areas attributes on LST_{ART}

The regression model regarding the effect of herbaceous patches on LST of non-vegetated patches highlighted a significant relationship between LST_{ART} and the predictors (P-value: $1.216x10^{-7}$, Fig. 3.8). Particularly, we found a significant negative relationship between TA_{HERB} and LST_{ART} (Tab. 3.2), meaning that lower LST_{ART} values were reached for higher values of TA_{HERB}, namely herbaceous patches cover within cells.

Tab. 3.2: statistical parameters of regression model between LST_{ART} and herbaceus areas attributes.

Predictor	Estimated coefficient	Standard error	t-value	p-value
~TA_{HERB}	-0.359	0.102	-3.524	**0.0009**
~NP_{HERB}	-0.0003	0.019	-0.017	0.987
~TA_{HERB}:NP_{HERB}	0.004	0.004	1.020	0.312

Limit of significance: p-value < 0.05

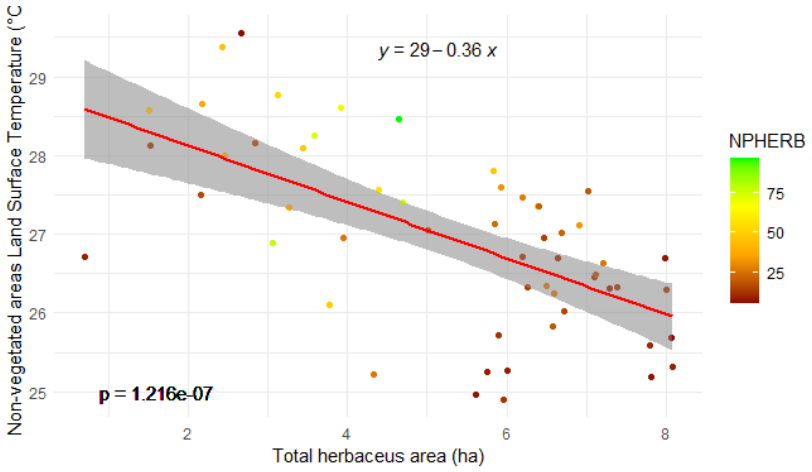

Figure 3.8: relathionship between LST_{ART} and the predictor variable TA_{HERB} (identifiable throught the abscissas line), NP_{HERB} (identifiable throught the colour gradient of the points), and TA_{HERB}*NP_{HERB} (identifiable trought the confidence band of the interaction).

Similarly, the regression model testing the influence of woody patches on LST of non-vegetated patches highlighted a significant relationship between LST_{ART} and the predictors (P-value: $1.529x10^{-5}$; Fig. 3.9). Particularly, we found a significant positive relationship between NP_{ARB} and LST_{ART} (Tab. 3.3), meaning that lower LST_{ART} values were reached for lower values of NP_{ARB}, namely with decrease in woody patches number within the cells.

Tab. 3.3: statistical parameters of regression model between LST_{ART} and woody areas attributes.

Predictor	Estimated coefficient	Standard error	t-value	p-value
~TA_{ARB}	-0.341	0.274	-1.245	0.219
~NP_{ARB}	0.055	0.022	2.522	**0.015**
~TA_{ARB}:NP_{ARB}	0.001	0.013	0.117	0.908
			Limit of significance: p-value < 0.05	

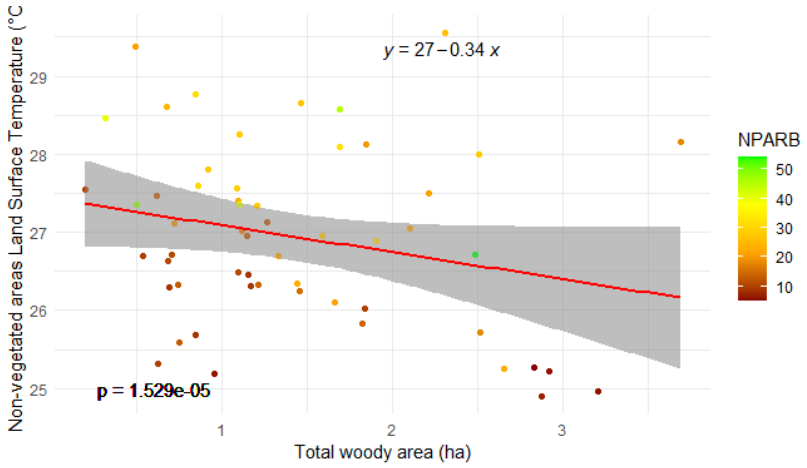

Figure 3.9: relathionship between LST_{ART} and the predictor variable TA_{ARB} (identifiable throught the abscissas line), NP_{ARB} (identifiable throught the colour gradient of the points), and TA_{ARB}*NP_{ARB}(identifiable throught the confidence band of the interaction).

Influence of woody and herbaceous total area ratio on LST_{ART}

The regression model about the influence of cover ratio among woody and herbaceous patches (TA_{ARB}/TA_{HERB}) on non-vegetated areas LST (LST_{ART}) did not show a significant relationship with the predictor variable (P-value > 0.05).

3.5 Cooling effect at patch level

The random selection of patches of the three considered land cover categories showed a high variability when considering their spatial attributes, thereby guaranteeing the necessary variability in configuration attributes to be met to answer the second research question.

At patch level, we found that urban green areas patches (i.e., highly managed herbaceous communities of suburban and industrial areas) had a mean patch area of 314.28 ± 949.1 m^2 ($AREA_{URB}$), a mean patch perimeter of 97.25 ± 94.84 m ($PERIMETER_{URB}$), and a mean shape index value of 1.91 ± 0.88 ($SHAPE_{URB}$) (Fig. 3.10 and Tab. 3.4).

Hedgerows patches had a mean patch area of 4646.25 ± 16838.54 m^2 ($AREA_{HED}$), a mean patch perimeter of 632.71 ± 1548.05 m ($PERIMETER_{HED}$), and a mean shape index value of 2.53 ± 1.22 ($SHAPE_{HED}$) (Fig. 3.11 and Tab.3.4). Finally, regarding seminatural grasslands patches we found a mean area of 8872.97 ± 8312.21 m^2 ($AREA_{GRA}$), a mean perimeter of 546.37 ± 290.26 m ($PERIMETER_{GRA}$), and a mean shape index value of 1.79 ± 0.53 ($SHAPE_{GRA}$) (Fig. 3.12 and Tab.3.4).

Tab. 3.4: mean attributes of the three land cover category.

Patch type	**Mean area (m^2)**	**Mean perimeter (m)**	**Mean shape index**
Urban green areas (i.e. highly managed herbaceous communities of suburban and industrial areas)	314.28 ± 949.1	97.25 ± 94.84	1.91 ± 0.88
Hedgerows	4646.25 ± 16838.54	632.71 ± 1548.05	2.53 ± 1.22
Grasslands	8872.97 ± 8312.21	546.37 ± 290.26	1.79 ± 0.53

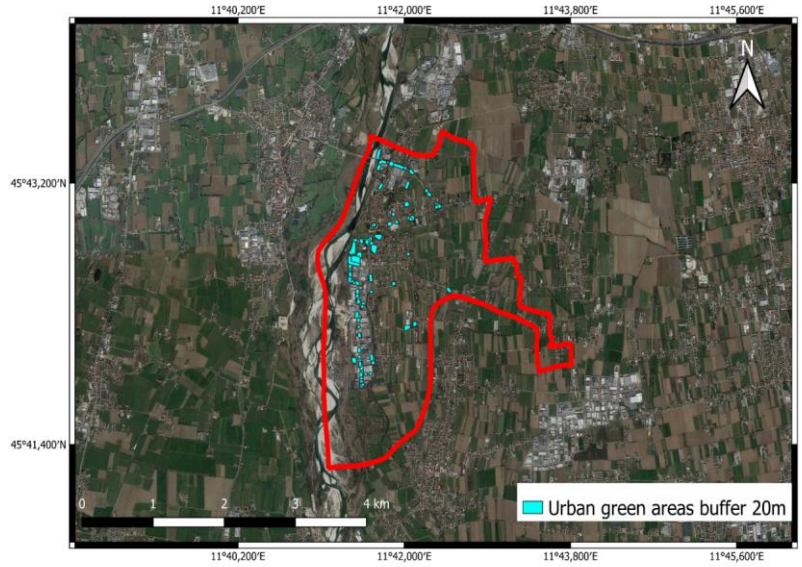

Figure 3.10: location of the chosen 100 urban green areas (i.e., highly managed herbaceous communities of suburban and industrial areas). Due to their limited surface, each patch has been enlarged through a 20m buffer to allow visualisation on the map.

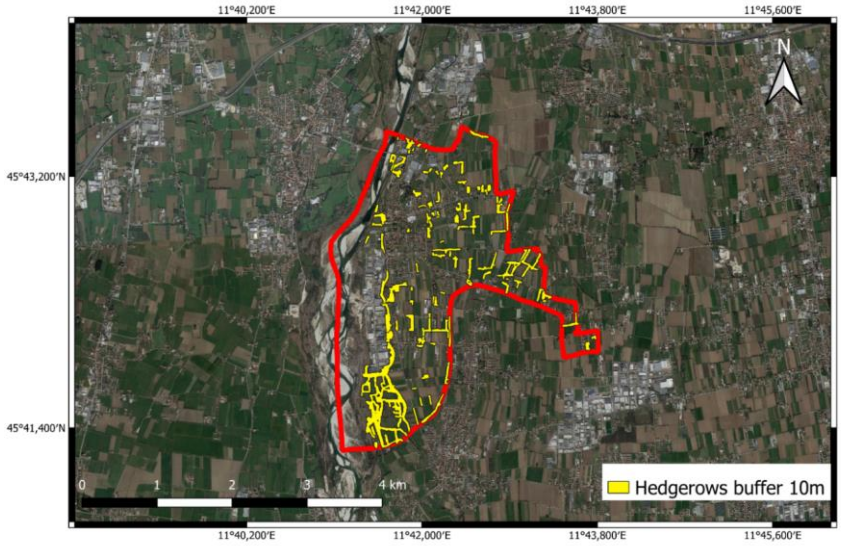

Figure 3.11: location of the chosen 100 hedgerows.

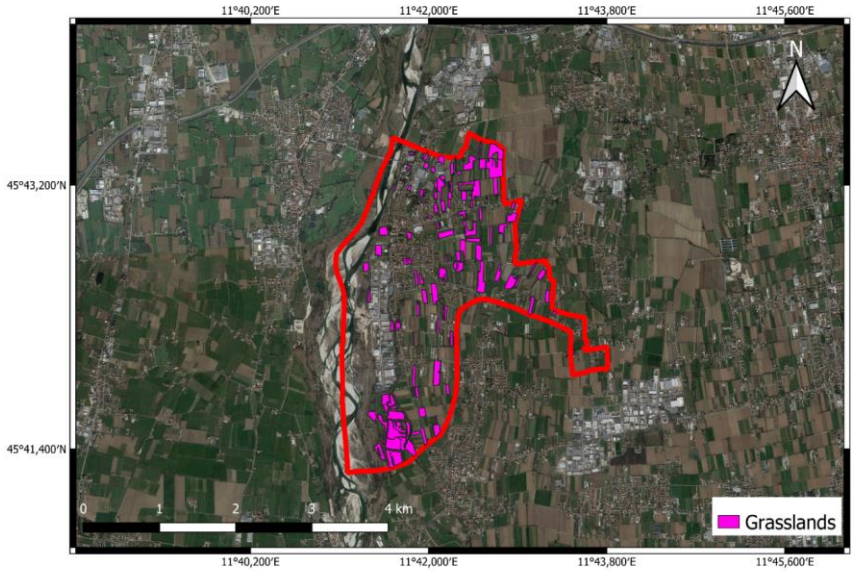

Figure 3.12: location of the chosen 100 grasslands.

Urban green areas, hedgerows, and grassland mean LST

The mean land surface temperature for urban green areas (LST_{URB}) resulted of 27.86 ± 1.20 °C, the mean LST for hedgerows (LST_{HED}) resulted of 26.18 ± 0.86 °C, and the mean land surface temperature for seminatural grasslands (LST_{GRA}) resulted 26.17 ± 1.02 °C.

Analysis of variance (ANOVA) revealed a significant difference among the three different considered categories (P-value: <2e-16; Fig. 3.13). Particularly, the post-hoc Tukey's HSD test highlighted significant LST differences between urban green areas and seminatural grasslands, and between urban green areas and hedgerows, with urban green areas exhibiting higher LST values in both cases (Tab. 3.5).

Tab. 3.5: statistical parameters of the Tukey's HSD test.

Group comparison	Difference	Lower	Upper	Adjusted p-value
LST_{GRA}-LST_{HED}	-0.214	-0.367	0.324	0.988
LST_{URB}-LST_{HED}	1.668	1.321	2.013	**0**
LST_{URB}-LST_{GRA}	1.689	1.345	2.034	**0**

Limit of significance: p-value < 0.05

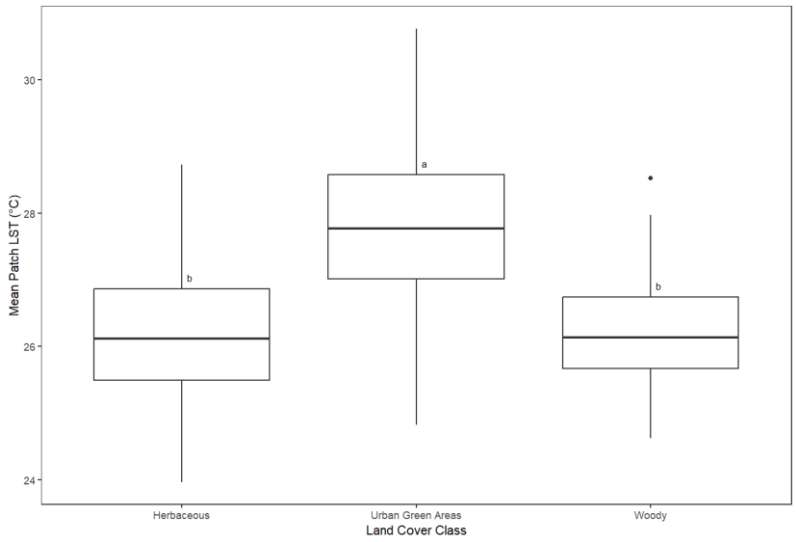

Tab. 3.13: Box plot obtained from the ANOVA and Tukey's test

LST of Urban green areas, hedgerows, and grasslands and the influence of their configurational attributes

The backward selection reduced the number of predictors in each regression model, revealing those variables involved in a significant relationship with the patches LST.

Specifically, backward selection in the linear regression model used to explain the relationships between LST_{URB} and predictors $AREA_{URB}$, $PERIMETER_{URB}$, and $SHAPE_{URB}$, showed that the shape index was the only predictor significantly related to LST_{URB} (Tab. 3.6). The negative value of the estimated coefficient suggests that more complex the shapes of urban green patches assure lower LST (Fig. 3.14).

The linear regression model used to assess the relationship between LST_{HED} and $AREA_{HED}$, $PERIMETER_{HED}$, and $SHAPE_{HED}$ highlighted that $PERIMETER_{HED}$ was the only predictor significantly related to patch LST_{HED} (Tab. 3.6). Particularly, the model revealed a negative value for the estimated coefficient for $PERIMETER_{HED}$, pointing out that hedgerows patches with greater perimeter showed lower LST values (Fig. 3.15).

Finally, backward selection applied to investigate the relationship between LST_{GRA} and $AREA_{GRA}$, $PERIMETER_{GRA}$, and $SHAPE_{GRA}$ revealed that $AREA_{GRA}$ was the only predictor significantly related to patch LST_{GRA} (Tab. 3.6). The negative value of estimated coefficient indicates that larger seminatural grasslands exhibited lower LST values (Fig. 3.16).

Tab. 3.6: statistical parameters of the regerssion models between LST of urban green areas, hedgerows, grasslands, and their configurational metrics.

Relationship	Estimated coefficient	Standard error	t-value	p-value
LST_{URB}~$SHAPE_{URB}$	-0.286	0.134	-2.13	**0.036**
LST_{HED}~$PERIMETER_{HED}$	-1.119×10^{-4}	5.366×10^{-5}	-2.085	**0.04**
LST_{GRA}~$AREA_{GRA}$	-3.436×10^{-5}	1.189×10^{-5}	-2.889	**0.005**
				Limit of significance: p-value < 0.05

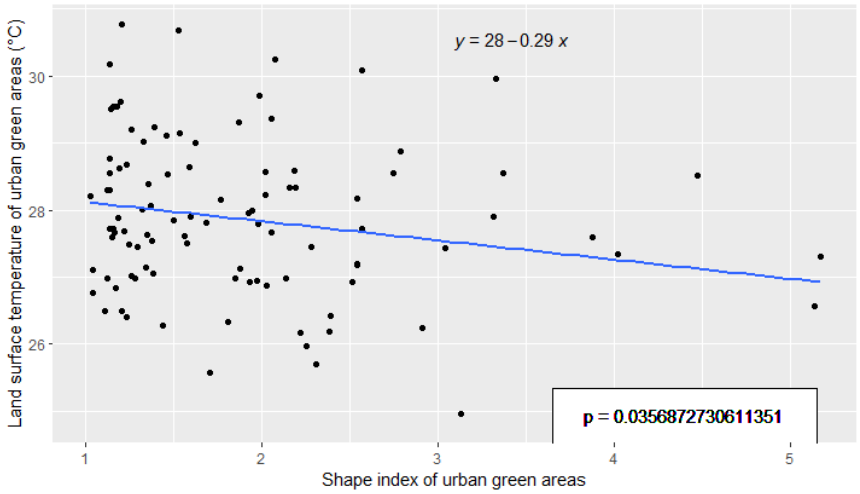

Figure 3.14: relathionship between LST_{URB} and $SHAPE_{URB}$

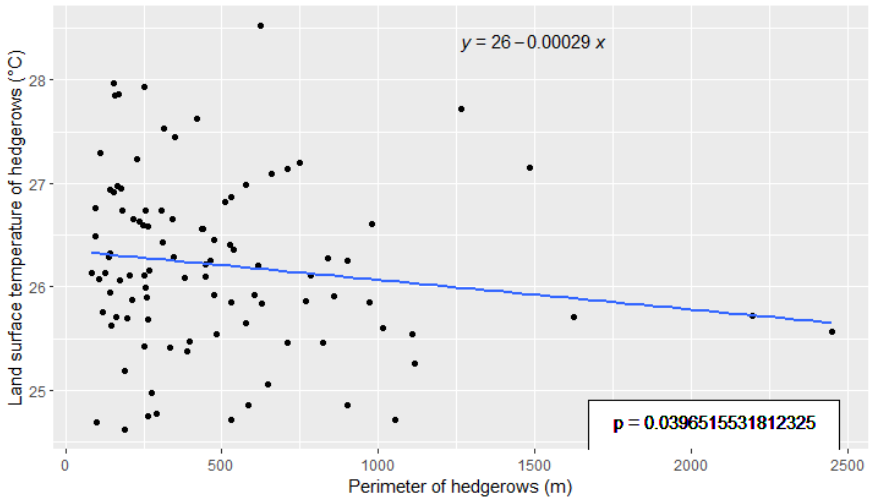

Figure 3.15: relathionship between LST_{HED} and $PERIMETER_{HED}$

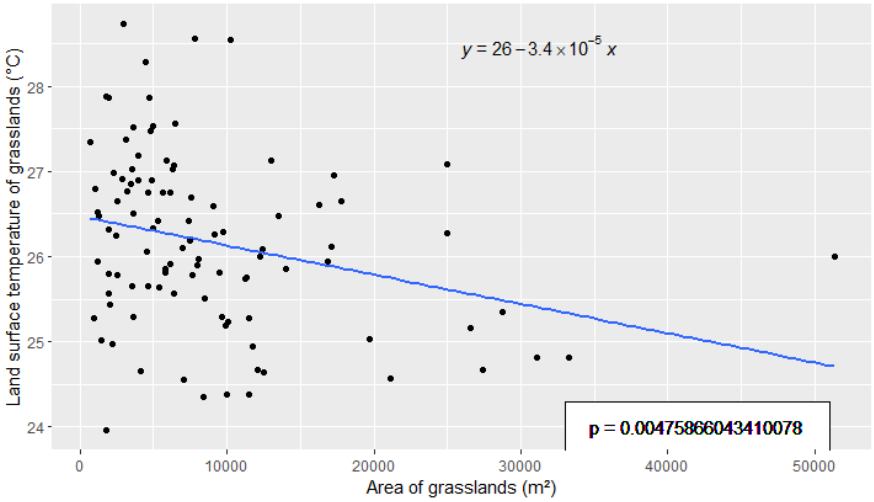

Figure 3.16: relathionship between LST_{GRA} and $AREA_{GRA}$

4 DISCUSSION

4.1 Landscape level highlights

In accordance with what pointed out by Mohajerani et al. (2017) for metropolitan city centres, we detected that higher extent of non-vegetated areas experienced higher temperatures.

Thanks to the high variability in vegetation cover analysed at landscape level, the results not only confirm the existence of a cooling effect provided by vegetation as indicated by Su et al. (2022) and Sugawara & Takamura (2014), but also prove that the supply of this ecosystem service is linearly linked to green area cover. This linear relationship can be traced back to the role of evapotranspiration in cooling effect, that can be considered an additive effect (Ma et al., 2019) that increases with increasing vegetation amount. Indeed, according to Su et al. (2022) a higher green cover would absorb a higher amount of local heat that would be loss as latent heat during evapotranspiration process. In this way, evapotranspiration affects local temperatures by making cooler those areas with more green area cover.

In contrast with Ode & Miller (2011), our results did not show a significant relationship between the number of green patches and the Land Surface Temperature of non-vegetated areas. Our contrasting finding could possibly be due to the greater influence of cover with respect to the number of patches within the performed model. Indeed, when the number of patches was combined with the total cover of green areas, the combined influence of both variables revealed to be significant and concurrent, i.e., the two variables affected the cooling effect in the same way. This means that, at the landscape level, more and bigger green area patches provide a higher supply of this ecosystem service, confirming the additive effect.

When considering green area types, namely “herbaceous patches” and “woody patches”, the results for the herbaceous areas followed the already discussed patterns found for the green areas *sensu lato*. Specifically, Land Surface Temperature of non-vegetated areas significantly decreased with increasing total area of herbaceous patches, while the number of patches resulted not significant. According to Zhang et al. (2009), this implies that a higher cover of herbaceous areas enhances the cooling effect supply. The opposite was revealed for woody areas, where the number of patches was the only significant variable related to Land Surface Temperature of non-vegetated areas that is, controversial to the observation for green areas, the cooling effect supply decrease with increased number of woody patches. Differently from previous studies (e.g., Zhang et al. 2009), we did not find any relationship between cooling effect and woody area cover. This is likely due to the linear shape

of most of woody patches in our study areas, that were mostly represented by hedgerows, rather than forests or other areal woody communities considered in previous studies. We hypothesise that due to their relatively narrow width, small and linear vegetation patches always have a longer perimeter compared to their internal surface; as such they are more likely subjected to the influence of neighbouring areas (a kind of edge effect) rather than influencing them. This hypothesis is in accordance with the observation of Zhang et al. (2009) for small green area patches in megacity contexts, where the Land Surface Temperature of non-vegetated areas decreased more slowly when the cover of vegetated patches became increasingly small. This effect can be also the cause for the absence of a significance when dealing with the woody and herbaceous total area ratio, where the role of woody cover might not have been appreciated in our study area. Moreover, due to the linear development of most of the woody patches, the considered ratio values might not be enough variable to fully comprehend the combined influence of herbaceous and woody green areas on cooling effect. In any case, as indicated by Masoudi et al. (2021) and Kowe et al. (2021), our results at landscape level highlight that fragmentation play a key role in reducing the supply for cooling effect, especially through cover reduction and increase in the number of small patches.

4.2 Patch level highlights

Our results highlighted a significant difference among the considered green area types. Particularly, urban green areas showed to be hotter than both hedgerows and seminatural grasslands, which in turns showed a similar Land Surface Temperature. The higher temperatures in urban green areas can be linked to both their mean surface and the context in which they are located. Although urban green areas and seminatural grasslands are both herbaceous communities, urban green areas usually have a limited surface compared to seminatural grasslands, making them prone to suffer from the effect of surrounding areas. Indeed, urban green areas are mostly located within the urban context, where the contrast with man-made elements is higher. Thus, the combined effect of a limited surface and the artificial context in which urban green areas are located can result in an intense edge effect, that in case of very limited surfaces can affect the whole patch, limiting their cooling capacity (Zhang et al., 2009). Moreover, the influence of (surrounding) high temperatures can enhance the evaporation of water from the soil, leading to a lack of water resources for plant growth and photosynthesis, worsening the depauperating of cooling effect (Su et al., 2022). Thus, green area patches not only influence the surrounding environment, but would be also affected by nearby elements, especially when of a different nature. The importance of the context in which green areas are located is confirmed by the absence of differences in Land Surface Temperature between seminatural grasslands and hedgerows. Seminatural grasslands and hedgerows are for the most part located in

rural areas where the degree of land artificialisation is low and green areas are mainly in contact with other green areas, thus making edge effect occurring weakly compared to what happens in greyer context (i.e., for urban green areas). Thus, the influence of the edge effect on temperatures of hedgerows and grasslands is mitigated because of similar nature of sides (Zhang et al., 2009).
Looking at patch configuration attributes, shape emerged to be the one significantly involved in explaining urban green areas temperatures. This result is in accordance with previous studies (e.g. LI et al., 2012), which suggested that urban green areas with a more complex shapes had a higher cooling capacity. However, there is still a lot of controversy surrounding this issue and different studies have produced diverging results and both compact and irregular shapes have been linked with better cooling. In our case, the major criticality regards the inconsistency with the results we found at landscape level for herbaceous areas, where results clearly indicated an additive effect of herbaceous patches, with LST values of artificial areas decreasing at increasing cover of herbaceous patches.
This inconsistency suggests that the mechanisms operating at the two different scale (landscape vs. patch level) are possibly different or the cooling capacity is modulated by other factors such as the context in which the patches are located. In addition, we cannot exclude methodological factors, e.g., data source and resolution, or metric selection that possibly give a different representation of the association between patch attributes and patch cooling capacity and supply (Li et al., 2023).

In line with the results about woody elements at landscape level, neither the surface nor the shape showed a significant influence on the Land Surface Temperature of hedgerows, being the perimeter the only patch attribute significantly involved in explaining their cooling capacity, namely, a longer perimeter determines a higher cooling capacity. Despite some previous studies pointed out an additive effect in the supply of this ecosystem service also for woody communities (Bihuňová et al., 2021), our results indicated that the area was not significant. These contrasting results might be attributed to the type of woody patches considered in the different studies. As stated above, woody patches of the study areas are mostly represented by hedgerows, with a typical linear development that might have overshadowed the role of the area in their cooling capacity. As the perimeter was the only attribute significantly related to Land Surface Temperature, the more elongated the shape, the greater the cooling capacity beside the possible edge effect that can be assumed equal among selected woody patches.

According to what found at landscape level, the Land Surface Temperature of seminatural grasslands revealed to be significantly influenced by their area, as underlined by previous studies on herbaceous communities (Kowe et al., 2021; LI et al., 2012). This result confirms the additive effect on the supply

of the cooling effect, with bigger seminatural grassland patches demonstrating a greater cooling capacity. Conversely, perimeter and shape were not found to influence grassland temperature. Contrary to hedgerows, the areal development of grassland elements led the area to be the prevailing attributes, thus obscuring the effects of perimeter. Moreover, differently from urban green areas, the average greater surface of seminatural grasslands, combined with their location, might be the reason for which shape was not relevant in cooling effect supply. Indeed, we suppose that influence of surrounding elements, i.e., the edge effect, is limited due to the greater extent of this elements (Zhang et al., 2009).

4.3 Cross scale evidence

Our results demonstrated that a cross-scale investigation allows a more exhaustive comprehension of the supply of cooling effect based on composition and configuration attributes at both landscape and patch level. Particularly, we highlighted that information on the supply of the investigated ecosystem service at different scale are complementary.

An interesting insight regards the herbaceous cover effect. At landscape level, we found that the LST of non-vegetated areas was significantly influenced by the total vegetation cover of herbaceous patches. This result could lead to believe that the effect of several small herbaceous patches is comparable to that of a lower number of larger patches, irrespective of each patch surface. However, the patch level analysis contributed to explain that the cooling capacity of each patch, and in turn its cooling effect, does depend on its surface; that is, larger patches have the capacity to maintain lower internal temperature; this in turn influences their cooling service supply. Interestingly, the cooling capacity of smaller patches of urban green areas revealed to be governed by patch shape rather than area, revealing more complex mechanism in the supply of this ecosystem service.

Thus, in summary, there is an additive effect of herbaceous patches, but the final cooling effect is modulated by the actual surface of patches, i.e., being equal the total cover, we should expect that the cooling capacity of a few larger patches would be higher than that of several small patches. Indeed, when patches become smaller, like urban green areas in our study area, the cooling process becomes more complex, entailing other patch attributes such as the shape.

Even woody elements revealed complementary insights while considering cooling effect at different scales. Particularly, a lower number of patches showed to improve the cooling effect at landscape level, while patch level analysis revealed that more elongated patches (i.e., higher perimeter values) have a greater cooling capacity. Indeed, hypothesizing a landscape where there is a unique long and continuous hedgerow, its cooling effect would be relatively hight because of its high perimeter, thus the Land Surface Temperature of surrounded non-vegetated areas would be relatively cold. In a same

landscape with numerous discontinued short hedgerows, its cooling effect capacity would be lower due to their shorter perimeter, thus the Land Surface Temperature of surrounded non-vegetated areas would be hotter.

Finally, the context in which green area patches are located revealed to influence green area cooling capacity and in turn their cooling effect. The importance of the context turned out to be particularly relevant for urban green patches, likely due to their usually small surface. As the surface decreases, the influence from the surrounding elements, namely the edge effect, can become so high to hamper the cooling capacity.

4.4 Useful insights

Based on the results of the cross-scale analysis, we provided new insights on the necessary requirements to be met by GI elements to maximize the supply of cooling effect. Considering that the planning of efficient GI is influenced by numerous conflicts of interest, due to limited resources (especially economic and spatial), these results allow to focus on those characteristics useful to make GI interventions sustainable.

The increase of temperature due to the reduction of green areas implies that GI elements should be primarily implemented in low vegetated areas as residential or industrial zones, where the cooling effect demand is higher. Green elements should be planned as to maximize their cover at landscape level, and minimising fragmentation of extant patches.

The inclusion of small green patches unlikely has significant results in terms of temperature reduction, especially in urban contexts, where artificialisation is high and new green patches are mostly in contact with impervious areas.

To assure GI efficacy, GI elements should be as large as possible to increase their cooling capacity and in turn the supply of the cooling effect. To overcome the issue regarding the limited space available for GI in urban context and solve the problem of the edge effect that can impair the supply of cooling effect, GI elements should be planned in combination to simulate the positive effect observed in rural areas. Our analysis suggest that cooling capacity can increase when herbaceous and woody elements are associated; in this regard, the efficacy of a small herbaceous area can be improved by adding an hedgerow bordering one or two sides of the patch.

5 REFERENCES

Tochaiwat, K., Phichetkunbodee, N., Suppakittpaisarn, P., Rinchumphu, D., Tepweerakun, S., Kridakorn Na Ayutthaya, T., & Sittisom, P. (2023). Eco-Efficiency of Green Infrastructure on Thermal Comfort of Outdoor Space Design. *Sustainability*, 15(3), 3566. https://doi.org/10.3390/su15032566

Li, X., Zhou, Y., Yu, S., Jia, G., Li, H., & Li, W. (2019). Urban heat island impacts on building energy consumption: A review of approaches and findings. *Energy*, 174, 407–419. https://doi.org/10.1016/j.energy.2019.02.183

Singh, N., Singh, S., & Mall, R. K. (2020). Urban ecology and human health: implications of urban heat island, air pollution and climate change nexus. In Verma, P., Singh P., Sinngh, R., Raghubanshi, A.S. (Eds) *Urban Ecology: Emerging Patterns and Social-Ecological Systems. Elsevier*, pp. 317–334. https://doi.org/10.1016/B978-0-12-820730-7.00017-3

Weng, Q., Lu, D., & Schubring, J. (2004). Estimation of land surface temperature-vegetation abundance relationship for urban heat island studies. *Remote Sensing of Environment*, 89(4), 467–483. https://doi.org/10.1016/j.rse.2003.11.005

Yan, C., Ding, J., Wang, B., Qin, L., Shi, Z., & Qiu, G. Y. (2023). An in-situ measurement and assessment of evaporative cooling effects of low impact development facilities in a subtropical city. *Agricultural and Forest Meteorology*, 332, 109363. https://doi.org/10.1016/j.agrformet.2023.109363

Heaviside, C., Macintyre, H., & Vardoulakis, S. (2017). The Urban Heat Island: Implications for Health in a Changing Environment. *Current Environmental Health Reports*, 4, 296–305. https://doi.org/10.1007/s40572-017-0150-3

Mohajerani, A., Bakaric, J., & Jeffrey-Bailey, T. (2017). The urban heat island effect, its causes, and mitigation, with reference to the thermal properties of asphalt concrete. *Journal of Environmental Management*, 197, 522–538. https://doi.org/10.1016/j.jenvman.2017.03.095

Jacobs, C., Klok, L., Bruse, M., Cortesão, J., Lenzholzer, S., & Kluck, J. (2020). Are urban water bodies really cooling? *Urban Climate*, 32, 100607. https://doi.org/10.1016/j.uclim.2020.100607

Grimmond, S. (2007). Urbanization and global environmental change: Local effects of urban warming. *Geographical Journal*, 173(1), 83–88. https://doi.org/10.1111/j.1475-4959.2007.232_3.x

Wai, C. Y., Muttil, N., Tariq, M. A. U. R., Paresi, P., Nnachi, R. C., & Ng, A. W. M. (2022). Investigating the relationship between human activity and the urban heat island effect in Melbourne and four other international cities impacted by COVID-19. *Sustainability*, 14(1), 378. https://doi.org/10.3390/su14010378

Yan, J., Zhao, L., Zhang, Y., & Zhang, L. (2022). Wind tunnel study on convective heat transfer performance of vegetation canopies with different structures. *Building and Environment*, 223, 109470. https://doi.org/10.1016/j.buildenv.2022.109470

Oke, T.R. (1974). Climatological effect. In *Review of urban climatology 1968-1973;* pp. 44-60; [Editor(s) unknown]; Geneva. https://library.wmo.int/doc_num.php?explnum_id=874

Ulpiani, G. (2021). On the linkage between urban heat island and urban pollution island: Three-decade literature review towards a conceptual framework. *Science of the Total Environment*. 751, 109363. https://doi.org/10.1016/j.scitotenv.2020.141727

Fahed, J., Kinab, E., Ginestet, S., & Adolphe, L. (2020). Impact of urban heat island mitigation measures on microclimate and pedestrian comfort in a dense urban district of Lebanon. *Sustainable Cities and Society*, 61, 102375. https://doi.org/10.1016/j.scs.2020.102375

Norton, B. A., Coutts, A. M., Livesley, S. J., Harris, R. J., Hunter, A. M., & Williams, N. S. G. (2015). Planning for cooler cities: A framework to prioritise green infrastructure to mitigate high temperatures in urban landscapes. *Landscape and Urban Planning*, 134, 127–138. https://doi.org/10.1016/j.landurbplan.2014.10.018

Elmqvist, T., Setälä, H., Handel, S. N., van der Ploeg, S., Aronson, J., Blignaut, J. N., Gómez-Baggethun, E., Nowak, D. J., Kronenberg, J., & de Groot, R. (2015). Benefits of restoring ecosystem services in urban areas. *Current Opinion in Environmental Sustainability*, 14, 101–108. https://doi.org/10.1016/j.cosust.2015.05.001

Su, Y., Wu, J., Zhang, C., Wu, X., Li, Q., Liu, L., Bi, C., Zhang, H., Lafortezza, R., & Chen, X. (2022). Estimating the cooling effect magnitude of urban vegetation in different climate zones using multi-source remote sensing. *Urban Climate*, 43, 101155. https://doi.org/10.1016/j.uclim.2022.101155

Sugawara, H., & Takamura, T. (2014). Surface Albedo in Cities: Case Study in Sapporo and Tokyo, Japan. *Boundary-Layer Meteorology*, *153*(3), 539–553. https://doi.org/10.1007/s10546-014-9952-0

Andrés-Anaya, P., Sánchez-Aparicio, M., del Pozo, S., & Lagüela, S. (2021). Correlation of Land Surface Temperature with IR Albedo for the Analysis of Urban Heat Island. *Engineering Proceedings*, *8*(1), 9. https://doi.org/10.3390/engproc2021008009

Tahooni, A., Kakroodi, A. A., & Kiavarz, M. (2023). Monitoring of land surface albedo and its impact on land surface temperature (LST) using time series of remote sensing data. *Ecological Informatics*, 75, 102118. https://doi.org/10.1016/j.ecoinf.2023.102118

Shadman, S., Ahanaf Khalid, P., Hanafiah, M. M., Koyande, A. K., Islam, M. A., Bhuiyan, S. A., Kok, S. W., & Show, P. L. (2022). The carbon sequestration potential of urban public parks of densely populated cities to improve environmental sustainability. *Sustainable Energy Technologies and Assessments*, 52, 102064. https://doi.org/10.1016/j.seta.2022.102064

Velasco, E., Roth, M., Norford, L., & Molina, L. T. (2016). Does urban vegetation enhance carbon sequestration? *Landscape and Urban Planning*, *148*, 99–107. https://doi.org/10.1016/j.landurbplan.2015.12.003

Zhang, Y., Meng, W., Yun, H., Xu, W., Hu, B., He, M., Mo, X., & Zhang, L. (2022). Is urban green space a carbon sink or source? - A case study of China based on LCA method. *Environmental Impact Assessment Review*, 94, 106766. https://doi.org/10.1016/j.eiar.2022.106766

Zhang, Q., Zhou, D., Xu, D., Cheng, J., & Rogora, A. (2022). Influencing factors of the thermal environment of urban green space. *Heliyon*, 8(11), 11559. https://doi.org/10.1016/j.heliyon.2022.e11559

Guo, G., Wu, Z., Xiao, R., Chen, Y., Liu, X., & Zhang, X. (2015). Impacts of urban biophysical composition on land surface temperature in urban heat island clusters. *Landscape and Urban Planning*, 135, 1–10. https://doi.org/10.1016/j.landurbplan.2014.11.007

Qiu, G. Y., Zou, Z., Li, X., Li, H., Guo, Q., Yan, C., & Tan, S. (2017). Experimental studies on the effects of green space and evapotranspiration on urban heat island in a subtropical megacity in China. *Habitat International*, 68, 30–42. https://doi.org/10.1016/j.habitatint.2017.07.009

European commission (2013). Green Infrastructure (GI) — Enhancing Europe's Natural Capital. {SWD (2013) 155 final}. https://eur-lex.europa.eu/resource.html?uri=cellar:d41348f2-01d5-4abe-b817-4c73e6f1b2df.0014.03/DOC_1&format=PDF

European commission (2021). Forging a climate-resilient Europe - the new EU Strategy on Adaptation to Climate Change. {SEC(2021) 89 final} - {SWD(2021) 25 final} - {SWD(2021) 26 final}. https://eur-lex.europa.eu/legal-content/EN/TXT/PDF/?uri=CELEX:52021DC0082

Mell, I. C. (2009). Can green infrastructure promote urban sustainability? *Proceedings of the Institution of Civil Engineers: Engineering Sustainability*, 162(1), 23–34. https://doi.org/10.1680/ensu.2009.162.1.23

Marando, F., Heris, M. P., Zulian, G., Udías, A., Mentaschi, L., Chrysoulakis, N., Parastatidis, D., & Maes, J. (2022). Urban heat island mitigation by green infrastructure in European Functional Urban Areas. *Sustainable Cities and Society*, 77, 103564. https://doi.org/10.1016/j.scs.2021.103564

Coutts, C., & Hahn, M. (2015). Green infrastructure, ecosystem services, and human health. *International Journal of Environmental Research and Public Health*, 12, 9768–9798. https://doi.org/10.3390/ijerph120809768

Heremans, S., De Blust, G., Suškevičs, M., K. Roche, P. (2021). Planning management for ecosystem service. In Suškevičs, M. and Roche, P.K. (Eds) *IMAGINE COOKBOOK SERIES N°4 Green Infrastructure management for ecosystem services*; pp. 46-60. 10.13140/RG.2.2.36061.33761

Capotorti, G., Valeri, S., Giannini, A., Minorenti, V., Piarulli, M., & Audisio, P. (2023). On the Role of Natural and Induced Landscape Heterogeneity for the Support of Pollinators: A Green Infrastructure Perspective Applied in a Peri-Urban System. *Land*, 12(2), 387. https://doi.org/10.3390/land12020387

Chen, D., Zhang, F., Zhang, M., Meng, Q., Jim, C. Y., Shi, J., Tan, M. L., & Ma, X. (2022). Landscape and vegetation traits of urban green space can predict local surface temperature. *Science of the Total Environment*, 825, 154006. https://doi.org/10.1016/j.scitotenv.2022.154006

Zhang, R. (2020). Cooling effect and control factors of common shrubs on the urban heat island effect in a southern city in China. *Scientific Reports*, 10(1), 17317. https://doi.org/10.1038/s41598-020-74559-y

Kowe, P., Mutanga, O., Odindi, J., & Dube, T. (2021). Effect of landscape pattern and spatial configuration of vegetation patches on urban warming and cooling in Harare metropolitan city, Zimbabwe. *GIScience and Remote Sensing*, 58(2), 261–280. https://doi.org/10.1080/15481603.2021.1877008

Zhang, X., Zhong, T., Feng, X., & Wang, K. (2009). Estimation of the relationship between vegetation patches and urban land surface temperature with remote sensing. *International Journal of Remote Sensing*, 30(8), 2105–2118. https://doi.org/10.1080/01431160802549252

Li, Y., Ren, C., Ho, J. Y. en, & Shi, Y. (2023). Landscape metrics in assessing how the configuration of urban green spaces affects their cooling effect: A systematic review of empirical studies. *Landscape and Urban Planning*, 239, 104842. https://doi.org/10.1016/j.landurbplan.2023.104842

Lindborg, R., Gordon, L. J., Malinga, R., Bengtsson, J., Peterson, G., Bommarco, R., Deutsch, L., Gren, A., Rundlof, M., & Smith, H. G. (2017). How spatial scale shapes the generation and management of multiple ecosystem services. *Ecosphere*, 8(4), 01741. https://doi.org/10.1002/ecs2.1741

Jones, S., & Somper, C. (2014). The role of green infrastructure in climate change adaptation in London. In *Geographical Journal*, 180, 191–196. Blackwell Publishing Ltd. https://doi.org/10.1111/geoj.12059

Matthews, T., Lo, A. Y., & Byrne, J. A. (2015). Reconceptualizing green infrastructure for climate change adaptation: Barriers to adoption and drivers for uptake by spatial planners. *Landscape and Urban Planning*, 138, 155–163. https://doi.org/10.1016/j.landurbplan.2015.02.010

De la Sota, C., Ruffato-Ferreira, V. J., Ruiz-García, L., & Alvarez, S. (2019). Urban green infrastructure as a strategy of climate change mitigation. A case study in northern Spain. *Urban Forestry and Urban Greening*, 40, 145–151. https://doi.org/10.1016/j.ufug.2018.09.004

European Commission (2012). The Multifunctionality of Green Infrastructure. Science for Environment Policy,| In-depth Reports. DG Environment. https://www.europarc.org/wp-content/uploads/2017/02/Green_Infrastructure.pdf

Salomaa, A., Paloniemi, R., Kotiaho, J. S., Kettunen, M., Apostolopoulou, E., & Cent, J. (2017). Can green infrastructure help to conserve biodiversity? *Environment and Planning C: Government and Policy*, 35(2), 265–288. https://doi.org/10.1177/0263774X16649363

Harrison, P. A., Berry, P. M., Simpson, G., Haslett, J. R., Blicharska, M., Bucur, M., Dunford, R., Egoh, B., Garcia-Llorente, M., Geamănă, N., Geertsema, W., Lommelen, E., Meiresonne, L., & Turkelboom, F. (2014). Linkages between biodiversity attributes and ecosystem services: A systematic review. *Ecosystem Services*, 9, 191–203. https://doi.org/10.1016/j.ecoser.2014.05.006

Soulé, M. E., Mackey2, B. G., Recher3, H. F., Williams4, J. E., & Woinarskj5, J. C. Z. (2004). The role of connectivity in Australian conservation. *Pacific Conservation Biology,* 10(4), 266 – 279. https://doi.org/10.1071/PC040266

Bocchiola, D., Nana, E., & Soncini, A. (2013). Impact of climate change scenarios on crop yield and water footprint of maize in the Po valley of Italy. *Agricultural Water Management*, 116, 50–61. https://doi.org/10.1016/j.agwat.2012.10.009

Goldblatt, R., Addas, A., Crull, D., Maghrabi, A., Levin, G. G., & Rubinyi, S. (2021). Remotely sensed derived land surface temperature (Lst) as a proxy for air temperature and thermal comfort at a small geographical scale. *Land*, 10(4), 410. https://doi.org/10.3390/land10040410

Sun, Z., Wang, Q., Batkhishig, O., & Ouyang, Z. (2016). Relationship between Evapotranspiration and land surface temperature under energy- and water-limited conditions in dry and cold climates. *Advances in Meteorology*, 2016, 1835487. https://doi.org/10.1155/2016/1835487

Stathopoulou, M., & Cartalis, C. (2007). Daytime urban heat islands from Landsat ETM+ and Corine land cover data: An application to major cities in Greece. *Solar Energy*, 81(3), 358–368. https://doi.org/10.1016/j.solener.2006.06.014

Tucker, C. J. (1979). Red and Photographic Infrared l,lnear Combinations for Monitoring Vegetation. *Remote Sensing of Environent*, 8, 127-150. https://www.sciencedirect.com/science/article/abs/pii/0034425779900130

Yu, X., Guo, X., & Wu, Z. (2014). Land surface temperature retrieval from landsat 8 TIRS-comparison between radiative transfer equation-based method, split window algorithm and single channel method. *Remote Sensing*, 6(10), 9829–9852. https://doi.org/10.3390/rs6109829

Al-Shaar, W., Bonin, O., Faour, G., Zeidan, N., & Al-Shaar, M. (2022). Spatial analysis of land surface temperature distribution: case of the Greater Beirut Area. *Euro-Mediterranean Journal for Environmental Integration*, *7*(4), 483–495. https://doi.org/10.1007/s41207-022-00330-6

Maeland, E. (1988). On the Comparison of Interpolation Methods. *IEEE Transiction on Medical Imaging*, 7, 213-217. https://ieeexplore.ieee.org/abstract/document/7784?casa_token=cCV3PvFaWokAAAAA:QakD_rBtYOPDrFLLLyOf8sCKlZFERwBvPsTQXg6nHFkFFLOEhTa4SV37TiJH5BprG5keDh03X1Yf

Aslam, W., Khurshid, K., Khan, A. A., & Karachi, P. (2016). Optimized Image Scaling Using DWT and Different Interpolation Techniques Space and Upper Atmosphere Commission. *International Journal of Advanced Computer Science and Applications*, 7, 294-300. https://scholar.google.com/scholar?hl=it&as_sdt=0%2C5&q=Optimized+Image+Scaling+Using+DWT+and+Different+Interpolation+Techniques+Space+and+Upper+Atmosphere+Commission&btnG=

McGarigal, K., & Marks, B. J. (1995). FRAGSTATS: spatial pattern analysis programme for quantifying landscape structure. U.S. Departement of Agriculture, Forest Servaice, Pacific Northwest Research Station; Portland. https://books.google.it/books?hl=it&lr=&id=FsI_GzPd5UUC&oi=fnd&pg=PA26&dq=McGarigal,+K.,+%26+Marks,+B.+J.+(1995).+FRAGSTATS:+spatial+pattern+analysis+programme+for+quantifying+landscape+structure&ots=ZYvxkii1zK&sig=ODE-L-I7kPfmbg2lpjSOv2E1UhA&redir_esc=y#v=onepage&q&f=false

Kovacevic, B., Djurovic, Z., Barrosa, V. (2000). QQ-plot based probability density function estimation. *Proceedings of the Tenth IEEE Workshop on Statistical Signal and Array Processing IEEE, 2000*, 243-247. https://ieeexplore.ieee.org/abstract/document/870120?casa_token=t6Sf9n6YdqsAAAAA:7g_sAVzZKZZkOJNxq3WdP_o27AIQrCISUSJI7pUOk7W5DC5GFJewcedjXeK8VZkIKvfSqb0YPHfp

Abdi, H., & Williams, L. J. (2010). Tukey's Honestly Significant Difference (HSD) Test. *Encyclopedia of Research Design*, 3(1), 1-5. http://www.utd.edu/~herve

Nanda, A., Mohapatra, Dr. B. B., Mahapatra, A. P. K., Mahapatra, A. P. K., & Mahapatra, A. P. K. (2021). Multiple comparison test by Tukey's honestly significant difference (HSD): Do the confident level control type I error. *International Journal of Statistics and Applied Mathematics.* 6(1), 59-65. https://doi.org/10.22271/maths.2021.v6.i1a.636

Ma, Z., Yan, N., Wu, B., Stein, A., Zhu, W., & Zeng, H. (2019). Variation in actual evapotranspiration following changes in climate and vegetation cover during an ecological restoration period (2000–2015) in the Loess Plateau, China. *Science of the Total Environment, 689*, 534–545. https://doi.org/10.1016/j.scitotenv.2019.06.155

Estoque, R. C., Murayama, Y., & Myint, S. W. (2017). Effects of landscape composition and pattern on land surface temperature: An urban heat island study in the megacities of Southeast Asia. *Science of the Total Environment*, *577*, 349–359. https://doi.org/10.1016/j.scitotenv.2016.10.195

Ode, Å., & Miller, D. (2011). Analysing the relationship between indicators of landscape complexity and preference. *Environment and Planning B: Planning and Design*, *38*(1), 24–38. https://doi.org/10.1068/b35084

Masoudi, M., Tan, P. Y., & Fadaei, M. (2021). The effects of land use on spatial pattern of urban green spaces and their cooling ability. *Urban Climate*, 100743, *35*. https://doi.org/10.1016/j.uclim.2020.100743

Li, X., Zhou, W., Ouyang, Z., Xu, W., & Zheng, H. (2012). Spatial pattern of greenspace affects land surface temperature: Evidence from the heavily urbanized Beijing metropolitan area, *Landscape Ecology*, *27*(6), 887–898. https://doi.org/10.1007/s10980-012-9731-6

Bihuňová, M., Supuka, J., Tóth, A., Šinka, K., & Kuczman, G. (2021). Urban Green Areas and Woody Plant Composition: Dwelling Space Quality Factor in the Klokočina Housing Estate. *Ekologia Bratislava*, *40*(1), 80–90. https://doi.org/10.2478/eko-2021-0010

6 ANNEXES

Annex 1: https://univeit-my.sharepoint.com/:x:/r/personal/876808_stud_unive_it/Documents/Annex%201=%20ARPAV%20Ros%C3%A0%20station%20data.xlsx?d=w4659a7e46aad4c5ea405ca84c930833d&csf=1&web=1&e=UMleCQ&nav=MTVfezMwREE2NkZDLUMzODAtNDMwNC04QzJBLUQ0RjgwNTRBRDdDMH0

Annex 2: https://we.tl/t-ClmE1gITI5

Annex 3: https://univeit-my.sharepoint.com/:x:/r/personal/876808_stud_unive_it/Documents/Annex%203=%20EUNIS%20categories%20attributes.xlsx?d=w36c6b100a2944cc9a5dd31836345673d&csf=1&web=1&e=c8l5iR&nav=MTVfezZBNUI4NkIxLTdDQzMtNDhBMC05RThGLUFBOTY5RjY4RDk3Rn0